Carl von Ossietzky Universität Oldenburg

Høgskulen på Vestlandet

Bachelor's degree in Environmental Sciences

Bachelor thesis

The effect of recent (0-80 years) environmental change on the geochemical (XRF and magnetic susceptibility) record of Lærdalsfjord sediments, Western Norway

Submitted by Sarah Vanessa Hartmann

First Supervisor: Prof. Dr. Matthias Paetzel (HVL)

Second Supervisor: Priv.-Doz. Dr. Holger Freund (UOL)

Oldenburg, 25.05.2023

Abstract

This thesis reconstructs past environmental change using the geochemical record of two sediment cores the Inner and Outer Lærdalsfjord, Western Norway. Reconstruction of past environmental change of the Lærdalsfjord can provide useful information to evaluate the general health status of the related aquatic environment.

X-ray fluorescence and magnetic susceptibility for each of the two fjord basins are analysed and linked to their respective sources.

These sources are (a) the garbage dumping at Raudberg between the 1950s and 1970s, (b) the construction of the Hydropower plants in Borgund (1974) and Stuvane (1988), (c) the building of the Fodnestunnel (from 1993 to 1995) and the Lærdalstunnel (from 1995 to 1999), and (d) the successive loss of the natural delta of the river Lærdalselv due to construction activity by using the rock masses from the tunnel buildings.

Effects are visible in the XRF record regarding marine organic matter (bromine), mineral matter (iron, titanium, manganese, and potassium) and pollutants (lead, copper, argon, and niobium). The magnetic susceptibility reveals the distribution of organic and mineral matter and supports the XRF interpretation.

A simple box model is developed illustrating and summarising the effects of local environmental change on the Lærdalsfjord sediments. This model might help responsible authorities in managing necessary measures.

Acknowledgments

I would like to thank my supervisor Matthias Paetzel for offering me the possibility to write this thesis at the HVL in Norway. A big thanks to his amazing support during field work, laboratory and dealing with all my struggles throughout the process of writing this thesis. Thank you for answering my million questions and most importantly, thank you for your trust in me. Writing this thesis was definitely more fun as it would have been without you. You rock!

I would also like to thank my supervisor in Germany, Holger Freund, who made this thesis possible by agreeing to be my supervisor at the University of Oldenburg and cooperating with the HVL. I would like to thank him for his great help with the formalities, as I could not have done it without him.

Another thank you goes to Leif Hauge, as he was a big help for my thesis by contributing his insider knowledge about his time living in Lærdal.

Thanks to the University of Bergen, allowing me to use their ITRAX Core scanner and special thanks to Hafli Haflidason, who helped me scanning those sediment cores in the first place.

Last but not least, I would like to thank all the *From Mountain to Fjord 2022* students for their help in field work and analysing additional data I could now use in my thesis. A big thanks goes to Amy Yang, as she kindly provided me her data from her thesis and her knowledge about diatoms which helped me in my thesis.

Table of Contents

List of Figures

1. Introduction

A fjord is the deepest form of an estuary and marks the transition area between land and open ocean. They are found among other in the mid to northern latitudes, such as Greenland or Norway and mark an exceptional landform (Bianchi et al. 2020, Syvitski et al., 1995). Their biochemical and physical features are unique, as they combine freshwater and marine characteristics. Since climate change is affecting biochemical gradients and organisms, fjords are vulnerable ecosystems (Bianchi et al., 2020).

Fjords are sensitive to anthropogenic impact and environmental change, and fjords represent high-resolution sedimentary archives (Bianchi et al., 2020).

Sediments can accumulate consistently within fjord basins. Thus, the sediment record provides continuous information about recent regional marine and terrestrial processes, as well as past climatic and environmental change back in time (Syvitski et al., 1995; Howe et al., 2010). To document these influences, the geochemical sediment record has become an effective tool for understanding past environmental and climatic change and predicting such change to the fjord ecosystem in the future (Syvitski et al., 1987; Syvitski et al., 1995; Howe et al., 2010).

For a better comparison and uniform evaluation of different water bodies, the EU (European Union) Water Framework Directive was implemented in 2000, providing classification standards and laws in terms of the quality assessment of inland surface waters, as well as transitional and coastal surface waters. This includes the Program of Measures (PoMs) to protect, maintain and restore water bodies to a good ecological and chemical status (European Commission, 2020).

Although not part of this classification system, the geochemical record of a fjord sediment does not only allow reconstructing environmental change from the past, but also allows assessments in terms of the past and current ecological and chemical health status of a fjord (Syvitski et al., 1987; Howe et al., 2010), adding an additional quality to the EU Water Framework Directive.

A well-established and low-cost method for analysing the geochemical sediment record is the usage of X-ray fluorescence (XRF) and magnetic susceptibility. Elemental proxies can be used to reconstruct the past and predict future changes within a fjord system in terms of environmental change (Rothwell et al., 2015). This geochemical analysis is used for various environmental analyses of fjord sediments worldwide (Rothwell et al., 2015) and is performed in the Lærdalsfjord for the study at hand.

The Lærdalsfjord is a south-eastern tributary of the Sognefjord in Western Norway (Figure 1a and 1b) and covers an area of 11.3 km^2. Even though the Lærdalsfjord is a part of the EU Water Framework Directive, there has been no classification of the Lærdalsfjord since the implementation of that framework (Paetzel, 2023, *personal communication*). Despite of this, the official classification of the Lærdalsfjord is marked as "good" environmental status by the County environmental authorities, which thus requires confirmation (Vann-nett, 2023).

Figure 1(a) and (b) Map of Lærdal and the Lærdalsfjord in Norway, including (c) locations in and around Lærdal (modified after Norgeskart.no).

During the last 80 years, the Lærdalsfjord was increasingly exposed to environmental change due to anthropogenic impact. Table 1 is listing four phases of events that most likely influenced the fjord environment throughout this period (locations illustrated in Figure 1c).

Table 1, Overview table of four phases of events in and around Lærdal between 1950 and 2000; the single locations are shown in Figure 1c.

Phase	Event	Reference
I	Dumping and burning of garbage at Raudberg from the 1950s to the middle 1970s	Leif Hauge (2023), *personal communication*
II	Construction of the Hydropower plants at in Borgund (1974) and Stuvane (1988)	Jensen et al. (2021) Østfold Energi (2023), Store Norske Leksikon (2023)
III	Construction of the Fodnestunnel (1993 to 1995) and Lærdalstunnel (1995 to 2000)	Johnson and Golmen (1992) Bjerknes et al. (2001)
IV	Gradual loss of the natural Lærdalselv delta, with the main infill since 1993 until 2000	Fylksarkivet.no, Porten.no, Norgeibilder.no

This thesis uses the geochemical sediment record to determine the influence of this regional environmental change (Table 1) on the marine environment of the Lærdalsfjord in Western Norway.

2. Objectives

The major aim of this thesis is to answer the question if the geochemical (XRF and magnetic susceptibility) record of Lærdalsfjord sediments allows reconstructing recent (0-80 years) environmental change. To be able to answer this question, the following three objectives are formulated:

2.1 *Do recent (0-80 years) surface sediments from the Lærdalsfjord show variations in their geochemical (XRF, magnetic susceptibility) composition?*

The term “recent” is defined in this thesis as 0 to 80 years back in time. According to Gjerdingen (2018), the linear sedimentation rate of the Inner Lærdalsfjord is on average 0.30 cm/year over the past 100 years, using the ^{210}Pb dating method and the ^{137}Cs horizon from the 1986 Chernobyl radioactive accident. This number represents a

minimum estimate as Gjerdingen et al. (2018) used a gravity corer for the sediment sampling that would compress the sediments during sampling. The sedimentation rates are thus expected to be somewhat higher in the unconsolidated recent surface sediments. Haflidason (2020) used the dating of Gjerdingen (2018) for a core-to-core correlation to determine sedimentation rates of 0.22 cm/year in a parallel core taken from the Inner Lærdalsfjord. Taking the dating of these long cores as a basis, the 20 to 30 cm long recent sediment cores of this thesis might cover a timespan representing the last 80 years. In addition to this long core dating, Yang (2023) estimated sedimentation rates for short sediment cores that were recovered parallel to the sediment cores of the thesis at hand, taken from the Inner and the Outer Lærdalsfjord. Yang (2023) used the method of Paetzel & Dale (2010) who related freshwater diatom peaks in fjord sediments to precipitation peaks of the area. The resulting sedimentation rates of Yang (2023) range from 0.27 to 0.38 cm/year in the Inner Lærdalsfjord, and from 0.27 to 0.32 cm/year in the Outer Lærdalsfjord.

X-ray fluorescence (XRF) is a tool in geochemistry to analyse sediment cores for various elements between the 3rd and 6th period from the periodic table, starting from an atomic number of Z=13 (Figure 14) in a time-saving and non-destructive way (Rothwell et al., 2015). XRF analysis indicates the different composition of sediments and allows a detailed analysis of the distribution of organic compounds (for example bromine as a proxy for marine productivity (Seki et al., 2019)) and inorganic compounds (for example lead, iron and manganese as proxies for pollutants and mineral matter input (Ahmed et al., 2013, Ren et al., 2009)).

Additionally, magnetic susceptibility can be used to support interpretations of elemental proxies and narrow down sources of errors (Kuhlmann et al., 2004, Møller et al. 2006). Thus, it is helpful to combine XRF and magnetic susceptibility for geochemical sediment analysis.

2.2 *Can changes within the geochemical sediment record resemble different phases of environmental change?*

Changes in mineral and organic matter content are expected due to known anthropogenic impact during the past 80 years.
Table 1 summarizes the major human induced impacts that occurred during the past 80 years. In addition, effects of climate change might have left traces in the sediment.

It is assumed that the Lærdalsfjord sediment cores show these environmental impacts in X-ray fluorescence and magnetic susceptibility, as generally documented for marine sediments when source areas of mineral material change (Croudace et al., 2006).

These four phases of environmental change (Table 1) are expected to have affected the geochemistry of the fjord, in addition to climate change. It is thus assumed to see changes within the geochemical record according to their respective source of environmental change. In this way, the geochemical record should allow to differentiate between these four phases of environmental change and link these geochemical changes of elements or element ratios to their respective phase of environmental change.

2.3 Is it possible to create an overview figure for the Inner and Outer Lærdalsfjord, illustrating their respective geochemical impacts by environmental change?

The Inner Lærdalsfjord is separated by a sill from the outer Lærdalsfjord and is directly influenced by the freshwater inflow from the river Lærdalselv, (Haflidason, 2020). The inner basin is directly exposed to anthropogenic impact, for example regarding the loss of the natural delta or the dumping of tunnel masses.

The Outer Lærdalsfjord is exposed to a different environmental setting as it is located more distant to the events happening in and around the Inner Lærdalsfjord (Haflidason, 2020). As a result, the Outer Lærdalsfjord is expected to be impacted less by environmental change, and the geochemical signals might thus differ within the geochemical sediment record between both fjord pools.

These differences within the geochemical record will be compared to each other and being visualized in a simple box model to point out the differences and similarities between the Inner Lærdalsfjord and the Outer Lærdalsfjord.

3. Environmental Setting

3.1 Bathymetry and Topography

The Lærdalsfjord is a side inlet of the Sognefjord and located approximately 130 km inland (Figure 1b) from the Norwegian west coast towards the east. According to Haflidason (2020), the Lærdalsfjord has a length of approximately 9 km, with a width of 2.3 km at its widest and 700 m at its narrowest part. A 46 m deep sill divides the Inner Lærdalsfjord basin from the Outer Lærdalsfjord basin (Figure 2c). The Inner Lærdalsfjord has a maximum water depth of 55 m, while the water depth of the Outer Lærdalsfjord exceeds 845 m below sea level (Haflidason, 2020). The tide in the Lærdalsfjord changes with an amplitude of 1 m to 1.5 m per tidal cycle (Haflidason, 2020).

There are two rivers entering the Lærdalsfjord. The river Erdalselv flows into the Outer Lærdalsfjord, while the mouth of the river Lærdalselv formed the delta at the easternmost shores of the Inner Lærdalsfjord (Figure 2b, norgeskart.no).

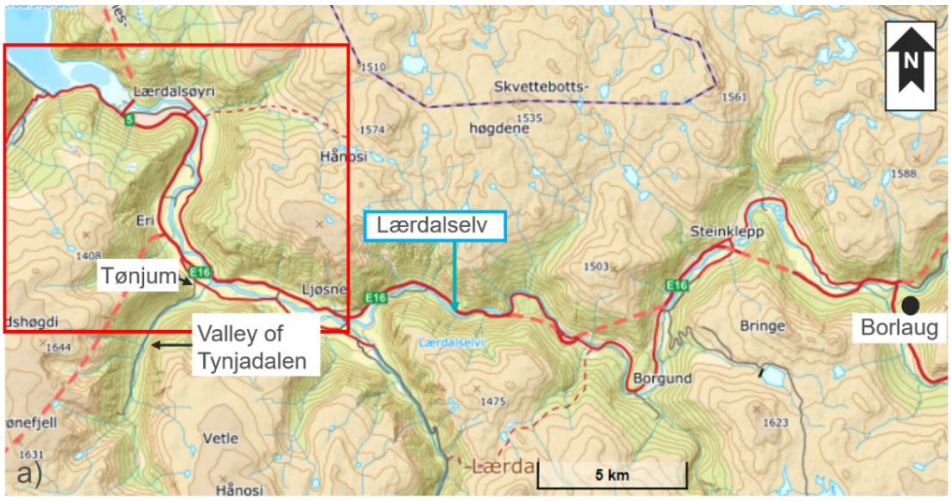
Lærdalsøyri
Skvettebotts-
høgdene
Hånosi
Eri
Lærdalselv
Steinklepp
Tønjum
Ljøsne
Valley of
Tynjadalen
Bringe
Borlaug
Borgund
Vetle
Lærdal
5 km
a)
N


b)
Fodnes
Lærdalsfjorden
Vetanosi
Fodnes-
tunnelen
Berdalen
Heste-
hovden
Delta
Grånosi
Lærdalsøyri
Oftedalen
Ofta
Sæbø
Helland
Tøri
Mjelde
Hunderi
Hauge
Erdalselv
Nyborg
Lærdalselv
Eri
Nordnosi
Molde
Såta
Tønjum
Øygard
Øvrevoll
Ljøsne
Grøte
Bø
Ytri
Tynjadalen
Valley of
Tynjadalen
Mouth of river
Erdalselv
Mouth of river
Lærdalselv
Mountains
2 km
N

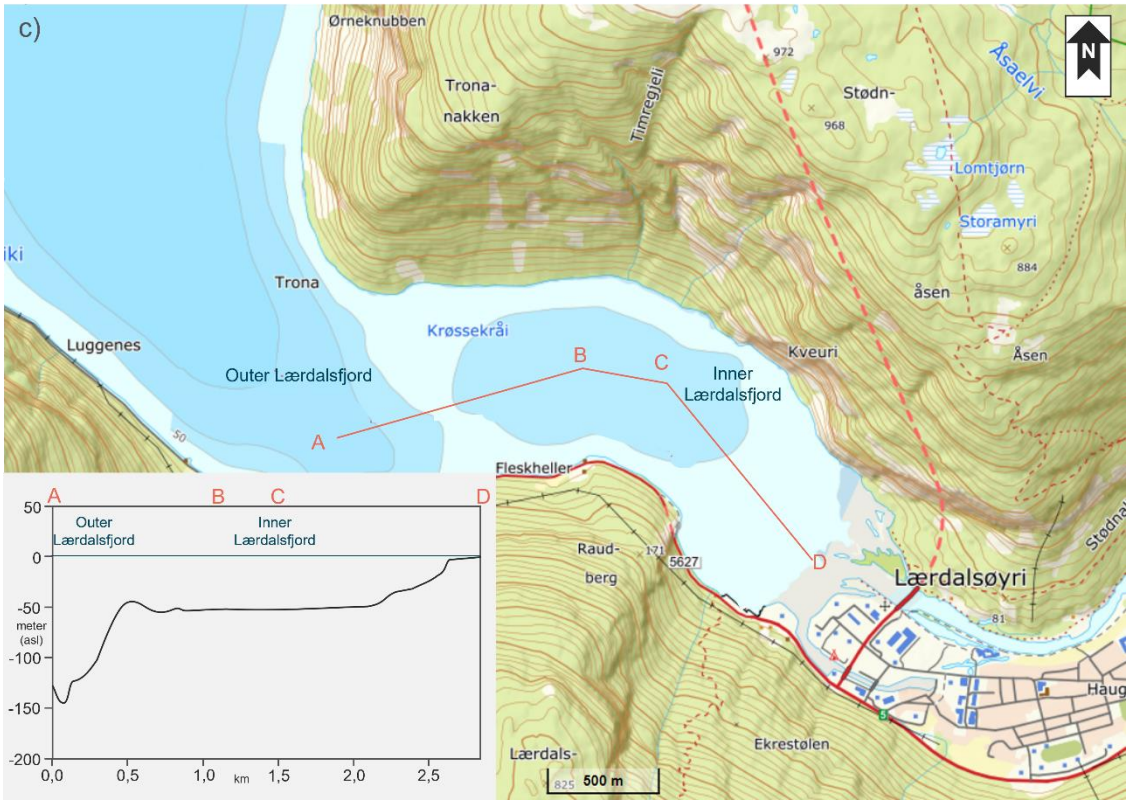

Figure 2, (a) Topographical map, showing the beginning and end of the river Lærdalselv. (b) Topographical map of the Inner and Outer Lærdalsfjord, showing the mouth of the river Erdalselv (dark blue arrow) and of the river Lærdalselv (light blue arrow), as well as the three mountains Vetanosi, Grånosi and Såta (Green box, modified after norgeskart.no). (c)(d) Bathymetry profile (modified after Yang, 2023). Straight orange lines and capital letters A, B, C, and D of Figure 2c correspond of the same letters and depth profile of Figure 2d.

The river Lærdalselv starts at Borlaug and has its mouth at the delta of the Inner Lærdalsfjord (Figure 2a, 2b, Gjerdingen, 2018). Furthermore, the river Lærdalselv contributes the most freshwater into the fjord system (Haflidason, 2020).

The Lærdalsfjord is surrounded by three mountains named Såta, Grånosi, and Vetanosi (Figure 2b). The mountain Såta is the highest with a height of 1409 m and located south of the Inner Lærdalsfjord, bordering the settlement of Tønjum and the valley Tynjadalen (Figure 2b, Norgeskart.no, Haflidason 2021). The mountain Grånosi is orientated southwest of the Lærdalsfjord and has a total height of 1209 m, while the mountain Vetanosi is located at the northern side of the Lærdalsfjord and is 1134 m high (Figure 2b, Norgeskart.no).

3.2 Hydrography

The Lærdalsfjord has a sill which works as a barrier between the Inner Lærdalsfjord basin and the open Outer Lærdalsfjord and is thus referred to as a silled fjord (Aksnes et al., 2019). In general, fjords provide a clear stratification (Stigbrandt, 2012), dividing the water column into three layers (Aksnes et al., 2019).

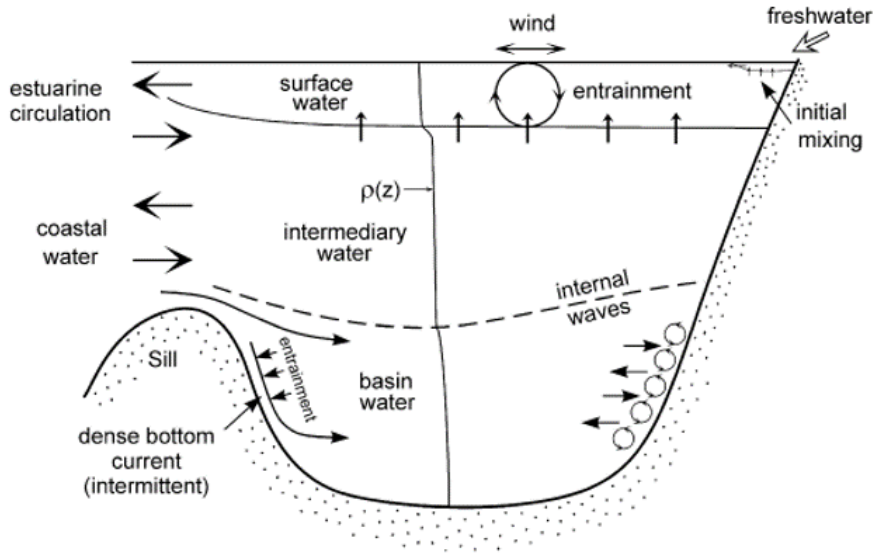

Figure 3, Model of the fjord circulation and fjord stratification (modified after Stigbrandt, 2012).

The top layer is the surface water (Figure 3, Aksnes et al., 2019, Stigbrandt, 2012). CTD measurements of the Inner Lærdalsfjord show a thickness of the top layer of 9 m, with salinity ranging from 0 to 26.77 PSU, temperature between 12.6 and 15.5°C, and oxygen ranging from 10 to 10.5 mgO_2/l (Figure 4, Torbjørn Dale 2023, *personal communication*). Furthermore, the top layer is formed by the supply of freshwater from rivers and runoff (Stigbrandt, 2012), which are the rivers Lærdalselv and Erdalselv, with the river Lærdalselv as main contributor (Haflidason, 2020).

The next, deeper layer is called the intermediary water (Figure 3) and its depths reaches from the bottom of the upper layer (9 m) downward to the sill depth at 46 m water depth. Salinity (from 27 to 34 PSU), temperature (between 12.5 and 10.5°C) and oxygen levels (from 9.6 to 8.5 mgO_2/l) indicate mostly uniform patterns within a small change (Figure 4, Torbjørn Dale 2023, *personal communication*).

The deepest layer, located below the intermediary water, is the basin water (Figure 3). In the Inner Lærdalsfjord, the basin water forms from 46 m downwards and has a salinity of 34 to 34.5 PSU, decreasing oxygen levels from 8.34 mg/l down to a minimum

of 3.87 mgO_2/l, and a temperature of 9°C (Figure 4, Torbjørn Dale 2023, *personal communication)*. The basin water is also the densest layer of all three water masses (Stigbrandt, 2012, Torbjørn Dale 2023, *personal communication*).

In addition to tidal currents, wind forces govern the surface currents as the surface currents usually equal the direction of the wind with a velocity of a fraction of the wind speed. Additionally, the wind also is affecting the estuarine circulation, as it allows vertical mixing of the surface layer (Figure 3). The estuarine circulation induces the surface water to flow out of the fjord, while the saline sea water flows into the fjord (Figure 3, Stigbrandt, 2012).

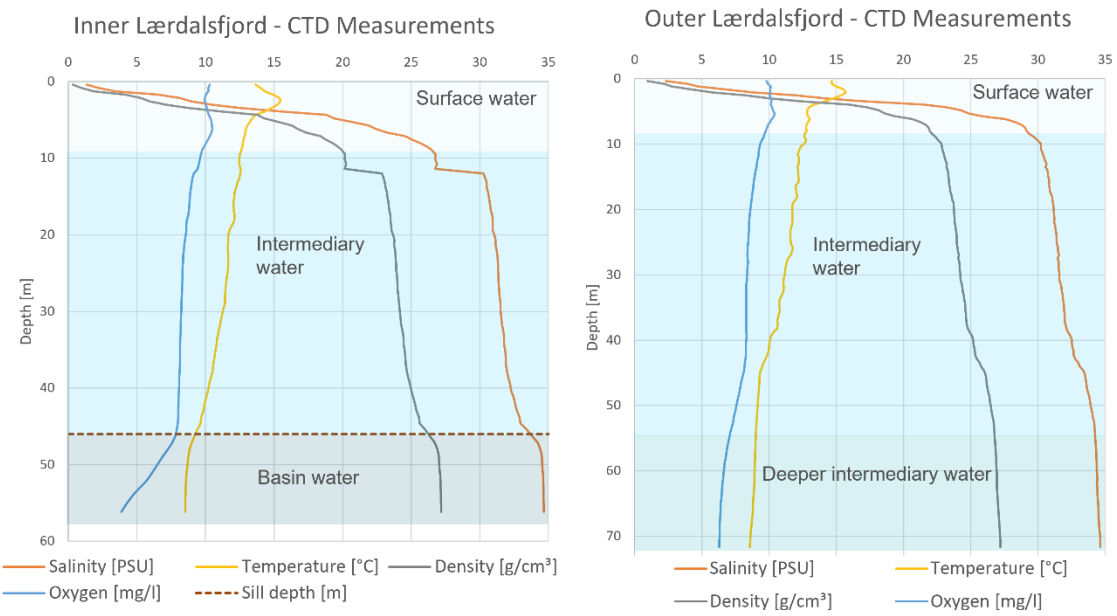

Figure 4, CTD (Conductivity, Temperature, Depth) measurements of the Inner and Outer Lærdalsfjord with the parameters salinity (orange), oxygen (blue), temperature (yellow) and density (grey). (Modified after Torbjørn Dale 2023, personal communication).

The outer Lærdalsfjord has its surface water between 0 to 8 m water depth with a salinity of 3 to 29 PSU, temperature ranging between 14 and 12.8°C, and oxygen concentration of 10 to 9 mgO_2/l (Figure 4, Torbjørn Dale 2023, *personal communication*).

The intermediary water is located between 8 and 45 m water depth. Salinity is around 29 to 33.5 PSU, temperature ranges between 12.7 and 9.3°C and oxygen concentrations are 9 to 8 mgO_2/l (Figure 4, Torbjørn Dale 2023, *personal communication*).

As the Outer Lærdalsfjord basin is deeper than the Inner Lærdalsfjord basin, the depth of the basin water is not reached within the CTD profiles. The layer from 46 m onwards is thus named a deeper intermediate water and indicated by an increase in salinity from 33.5 to 34.6 PSU and decreasing temperature from 9.3 to 8.5°C, and oxygen concentrations decreasing from 8 to 6 mgO_2/l (Figure 4, Torbjørn Dale 2023, *personal communication*).

Furthermore, according to the oxygen classification by Tyson and Pearson (1991) (Table 2), both fjord basins resemble an oxic environment with aerobic conditions.

Table 2, Oxygen classification, modified after Tyson & Pearson (1991). The oxygen concentration has been transformed from ml/l into mg/l. 1 ml equals 1.42 mg oxygen (Torbjørn Dale 2023, personal communication).

Oxygen ml/l	Oxygen mg/l	Oxygenation regime/ Environment Facies	Biofacies	Physiological regime
8.0 – 2.0	11.36 – 2.84	Oxic	Aerobic	Normoxic
2.0 – 0.2	2.84 – 0.284	Dysoxic	Dysaerobic	Hypoxic
2.0 – 1.0	2.84 – 1.42	moderate		
1.0 – 0.5	1.42 – 0.71	severe		
0.5 – 0.2	0.71 – 0.284	extreme		
0.2 – 0.0	0.284 – 0.0	Suboxic	Quasi-anaerobic	
0.0 (H_2S)	0.0	Anoxic	Anaerobic	Anoxic

3.3 Geology

According to the Norwegian Geological Survey (Norges Geologiske Undersøkelse, NGU), the dumped rock material from the Fodnestunnel (Table 3) includes Anorthosite and Anorthositic Gabbro, Gabbro, Granodiorite and Granite (Figure 5).

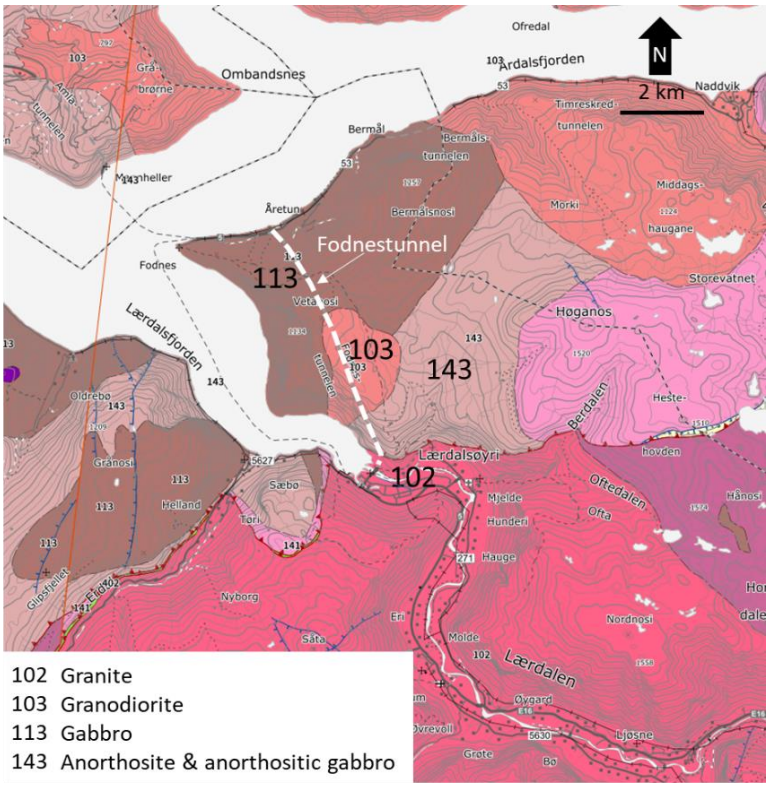

Figure 5, Overview map of the bedrock of the Fodnestunnel rock masses (modified after NGU.no)

Classifying the minerals of these rocks by using an IUGS diagramme after Streckeisen (1976, Gjelle et al., 1995, Le Maitre et al., 2002, Figure 6) shows the rocks (Anorthosite (green), Anorthosistic gabbro (green), Gabbro (green), Granodiorite (yellow), Granite (red)) main containments of potassium feldspar (Figure 6, left tip), plagioclase feldspar (Figure 6, right tip) and quartz (Figure 6, upper tip). However, each rock has a different composition of these three minerals. Thus, all six rock compositions are listed in Table 3, according to their IUGS classification after Streckeisen (1976).

Table 3, Minerals and their chemical composition of the rocks occurring in the rocks of the Fodnestunnel according to the geological map in Figure 5 according to Streckeisen (1976).

Rocks	Minerals	Chemical composition
Anorthosite (Mafic to ultramafic)	Ca-Plagioclase (>90%) Clinopyroxene (<10%) • Augite • Diopside • Hedenbergite	$CaAl_2Si_2O_8$ $(Ca,Na)(Mg,Fe,Al,Ti)(Si,Al)_2O_6$ $CaMgSi_2O_6$ $CaFeSi_2O_6$
Gabbro (Mafic to ultramafic)	(Ca) Plagioclase (about 50%) Clinopyroxene (about 50%)	*as above*
Anorthositic gabbro (Mafic to ultramafic)	Ca-Plagioclase (>50%) Clinopyroxene (<50%)	*as above*
Granite (Felsic)	(Ca,Na) Plagioclase (>30%) Potassium feldspar (>30%) Quartz (>30%) Biotite (<10%)	$(Ca,Na)Al_2Si_2O_8$ $(Na,K)AlSi_3O_8$ SiO_2 $K(Mg,Fe)_3(AlSi_3O_{10})(F,OH)_2$
Granodiorite (Felsic)	(Ca,Na) Plagioclase (65-90%) Similar portions of potassium feldspar and quartz (up to 35%)	*as above*

Based on the mineral composition of the different rocks from the Fodnestunnel, the felsic minerals (Granite, granodiorite) contain as main cations potassium and sodium next to silicon and aluminium. Meanwhile, the mafic to ultramafic rocks (Anorthosite, gabbro, anorthositic gabbro) contain as main cations calcium, magnesium and iron in addition to less silicon and aluminium (Gjelle et al., 1995).

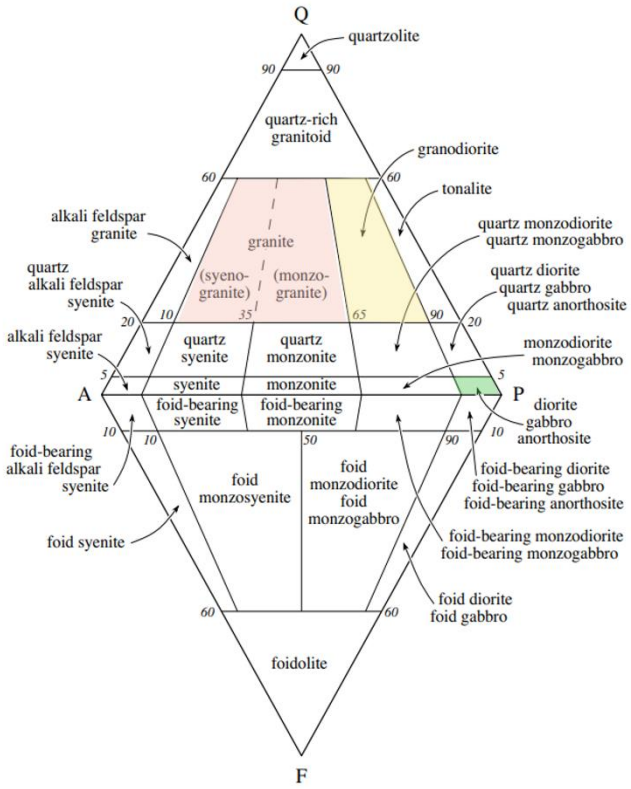

Figure 6, English version of the rock classification after Streckeisen (1976), highlighting the rock types from the surrounding bedrock around Lærdal (modified after Le Maitre et al., 2002).

3.4 Scientific Setting

A total of five investigations have been performed in the Lærdalsfjord during the last 40 years.

Johannessen and Lønning (1988) analysed the overall status of the Inner and Outer Lærdalsfjord, looking into hydrography, sediments and benthic invertebrates. They also looked into the impact of sewage water to the fjord environment and concluded that it does not cause any pollution to the fjord environment (Johannessen and Lønning, 1988).

Another research was conducted by the Norsk Institutt for Vannforskning, NIVA (Johnsen and Golmen, 1992). The research was arranged to assess potential locations for dumping tunnel masses from the planned construction of the Fodnestunnel and its potential impact on the fjord environment (Johnsen and Golmen, 1992).

In 2006, a survey was investigating the marine biology conditions in the Lærdalsfjord (Heggøy et al., 2007). It covers sedimentary and sea water analysis, as well as nutrients and the overall condition of benthic and littoral communities (Heggøy et al., 2007). Results stated a well oxygenated fjord with little nutrients and pollutants (Heavy metals, PAH, PCB) (Heggøy et al., 2007).

The first geochemical study was established during a Master thesis by Gjerdingen, 2018, who investigated flood events in the Lærdalsfjord and Aurlandsfjord in Western Norway over the past 2000 years.

The most recent study in the Lærdalsfjord was performed in 2020 to investigate the flood and deglaciation history of Western Norway (Haflidason, 2020). The Lærdalsfjord sediments were used to discover increasing flooding events for the last approximately 1120 years (Haflidason, 2020).

3.5 Historical Background

During the timespan of the past 80 years, the environment of Lærdal changed due to anthropogenic impact. The following subchapters provide an overview on those changes that most likely impacted the Lærdalsfjord environment (summary Table 1).

3.5.1 Garbage dumping at Raudberg

During the 1950s to 1970s, local farms and household burned their garbage at Raudberg. Additionally, garbage that could not be burned got dumped into the Lærdalsfjord at Raudberg (Leif Hauge, 2023, *personal communication*) (Figure 7a, 7b).

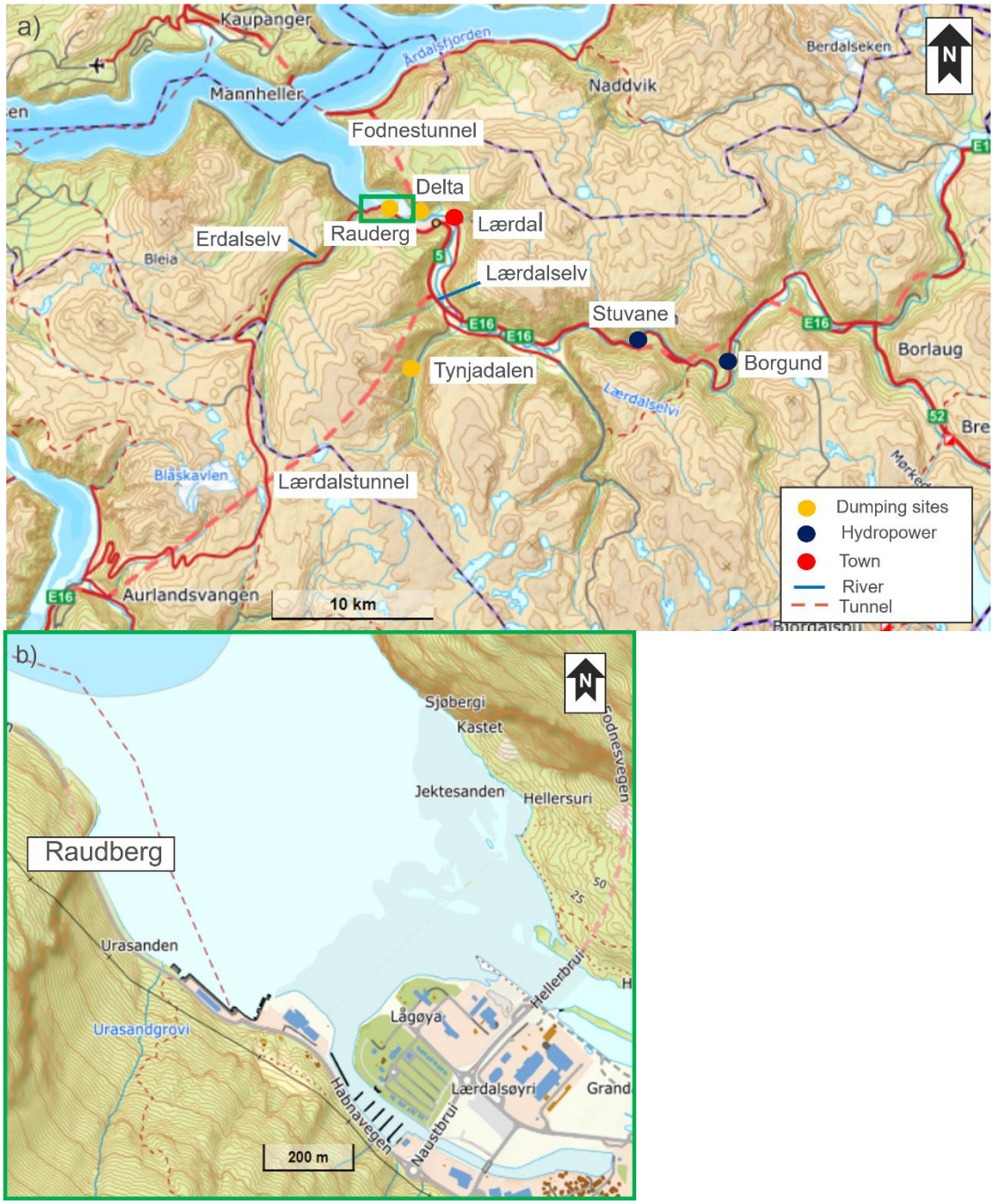

Figure 7,(a),(b) Location of garbage dumping and burning at Raudberg (modified after norgeskart.no).

The turning point of the garbage dumping marks the year 1974, as environmental policies came into focus. The Norwegian legislation adopted the environmental convention of the Nordic countries, and the new regulations came into action two years later on December 17th, 1976 (Klima- og miljødepartementet, 1976). Thus, environmental harassment was reduced from that date onwards, including the garbage dumping and burning in Lærdal. However, the exact year when the garbage dumping finally stopped is not documented.

Furthermore, it is indicated that the Raudberg site was used as a deposition place during construction of the Fodnestunnel for the material taken out of the tunnel. However, no official documentation on that could be found (Leif Hauge, 2023, *personal communication*).

3.5.2 Hydropower plants

The first hydropower plant was established at Borgund (Figure 8) and construction finished in 1974. The hydropower plant produces a mean capacity of 985 GWh annually (ØstfoldEnergi.no, 2023) by the river Lærdalselv.

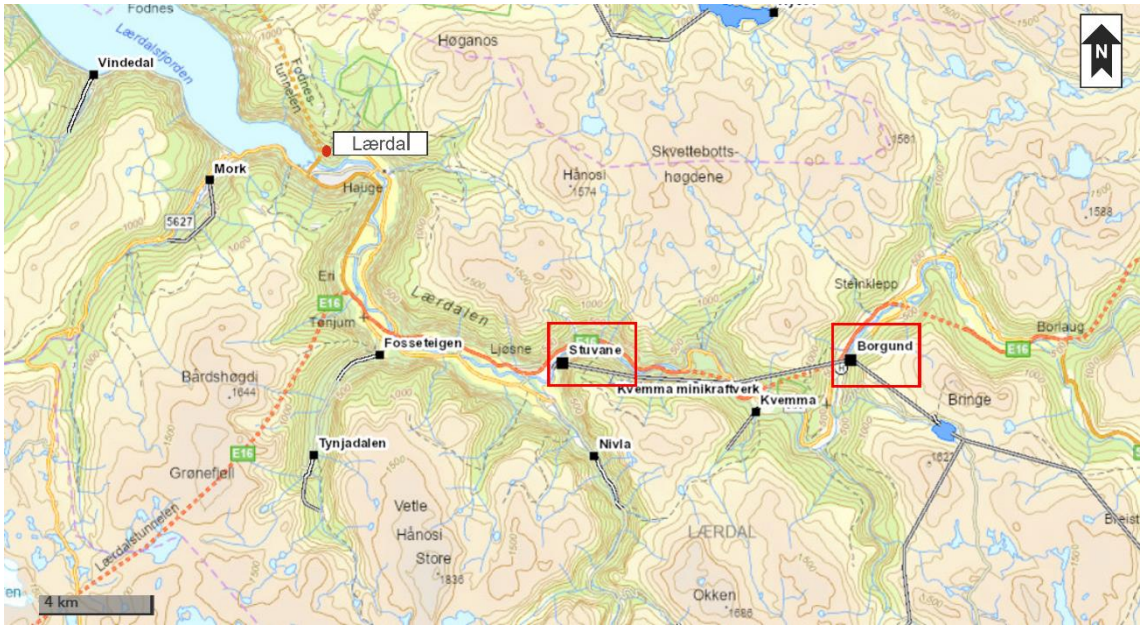

Figure 8, Location of Hydropower plants at Borgund and Stuvane (Modified after NVE.no). Straight double lines indicate the path the river water through water tunnels into the hydropower plants.

In 1988, a second hydropwer plant at Stuvane started operating. The hydropower plant at Stuvane is the hydropower station closest to the Lærdalsfjord (Figure 8). The water used for operating the hydropower plant is from the river Lærdalselv, hence it is using the same water as the station at Borgund. The mean annual capacity of the hydropower plant at Stuvane is 165 GWh (Jensen et al., 2021, Store Norske Leksikon.no, 2023).

3.5.3 The Fodnestunnel

The Fodnestunnel was built within a period of two years and connects the Sandnes peninsula (Figure 9a, black dot) with Lærdal. Construction started at 01.01.1993 and ended 31.12.1994. In total, rock material of 550 000 m^3 accumulated during the entire phase of construction (Johnson and Golmen, 1992), including the rock types of gabbro, granite, and anorthosite (Table 3).

These rock masses were being dumped at three different locations along the Lærdalsfjord (Figure 9c, stars), as suggested by Johnson and Golmen (1992).

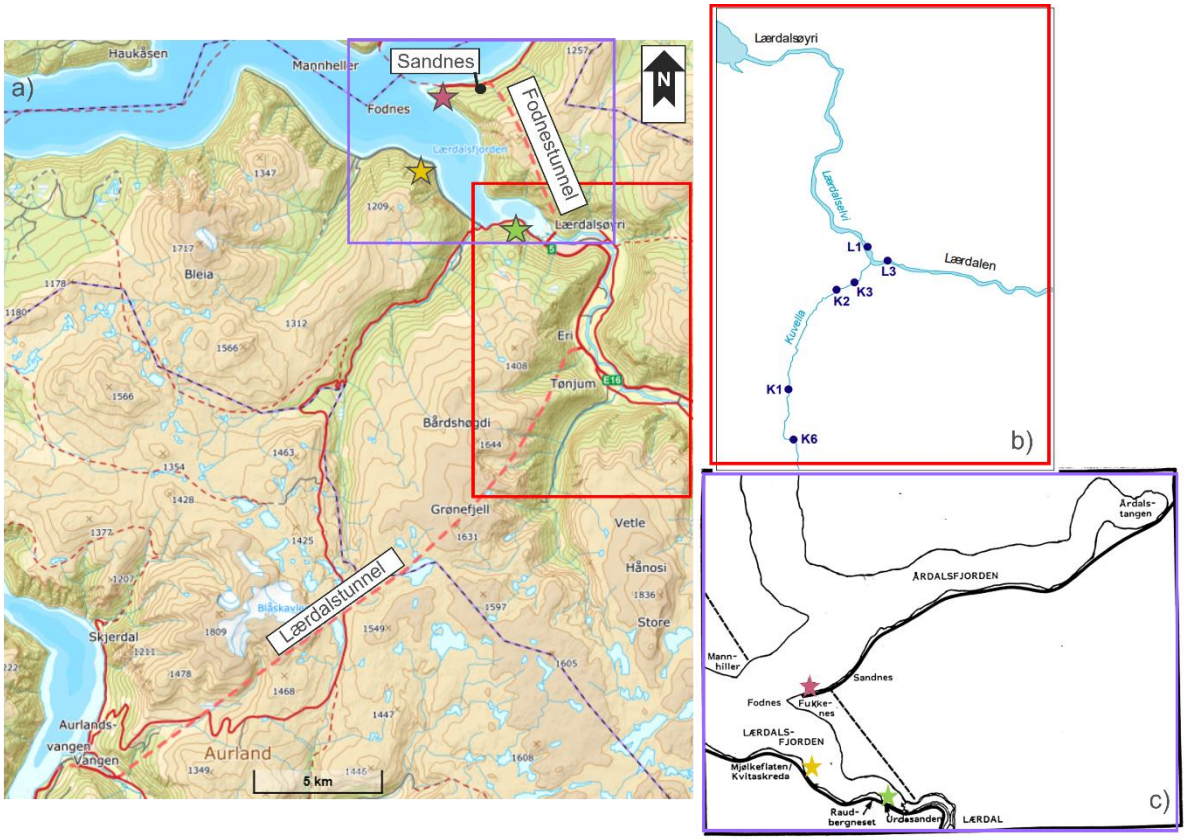

Figure 9, (a) Location of the Fodnestunnel and the Lærdalstunnel (modified after norgeskart.no). (b) Sampling locations (K1-K3, K6, L1, L3) for the conducted survey between 1996 and 1999 (Bjerknes et al., 2021). (c) Dumping locations (red, yellow green stars) for rock material from the Fodnestunnel (modified after Johnson et. al, 1992).

A total of 400 000 m^3 of rock material were dumped between Fodnes and Sandnes, (Figure 9a and 9c, red star).

Rock masses up to 300 000 m^3 were dumped at Mjølkflaten/Kvitaskreda, which is located roughly 3 km west alongside the Lærdalsfjord (Figure 9a and 9c), yellow star).

Finally, up to 150 000 m^3 were dumped between Urdasanden and Raudebergneset (Figure 9a and 9c, green star) (Johnson and Golmen, 1992).

Johnson and Golmen (1992) also addressed possible problems such as the dumped rock material being transported by the water current or the risk of increased turbidity. Another risk is the increase of nitrate levels after the rock dumping, as the explosive material contains nitrate binding containments (Johnson and Golmen, 1992).

3.5.4 The Lærdalstunnel

A major project in Western Norway was the construction of the Lærdalstunnel. With a length of 24.5 km, it is the longest tunnel in Norway (Statens vegvesen, 2023). The construction started in 1995 parallel to the valley of Tynjadalen, and the tunnel was completed in 1999, connecting the municipalities of Aurland and Lærdal (Figure 9a) (Bjerknes et al., 2001, Statens vegvesen, 2023). A total of 1.5 million m^3 of rock material was taken out and deposited and dumped in the valley of Tynjadalen near Tønjum (Figure 9a).

Research was conducted to investigate possible effects on the current water quality, flora, and fauna of the river Lærdalselv and the river Kuvella (Figure 9b) before construction started between in 1995.

During the construction period from 1996 to 1999, samples from six different locations alongside the river Lærdalselv and the river Kuvella (Figure 9b) have been analysed for chemical, physical and bacteriological parameters monthly (Bjerknes et al., 2001). The results of these analyses were within the natural variation range. The only exception were slightly increased nitrogen levels. However, the nitrogen levels decreased after the tunnel construction was finished in 2000. This concludes that those increased nitrogen levels were most likely due to contamination by the used explosive material.

After the building of the Lærdalstunnel was finished and the dumping of construction material stopped, nitrogen levels were still increased in the water column of the river Kuvella. Furthermore, the composition of the bottom fauna changed in the river Lærdalselv close to the outlet of the river Kuvella. This is most likely caused by the rock dumping from the Tynjadalen deposition site, leading to a change in rock particles settling onto the sediment (Bjerknes et al., 2001).

3.5.5 Loss of the natural delta

During the construction of the Fodnestunnel between 1993 and 1995 (Johnson and Golmen, 1992), rock material from the tunnel got also deposited on the delta and used for the delta re-build itself (Fylksarkivet i Vestlandt.no). Thus, construction of the delta re-built started simultaneously as the Fodnestunnel was built. The construction plan from 1991 from the archive of the municipality of Lærdal (Appendix 1, Lærdal municipality (1991)) shows the planned re-built of the delta in Laerdal to the year 1995, including finished constructions of the Fodnestunnel and the new established road nearby.

According to the construction plan from 1995 (Appendix 2, Lærdal municipality (1995)), the western part of the new established road into the area *Grandane* of the delta was planned.

The construction plan from 2005 (Appendix 3) indicates this build-up and shows further plans, including the expansion of the delta at the northwest end which were built until 2008 (Lærdal municipality (2005)).

Furthermore, satellite images from 1961 to 2022 (Figure10a-c) show how the delta evolved during the years. While the image from 1961 (Figure 10d) shows the delta in its almost natural state, the image from 1981 (Figure 10c) already shows the beginning of cultivation of the delta area, which continues until 2008. The satellite images from 2006 and 2022 (Figure 10a, 10b) indicate the delta being completely cultivated. It is assumed that the delta cultivation already began in the mid-1970s with its main construction activity from 1993 to 2008.

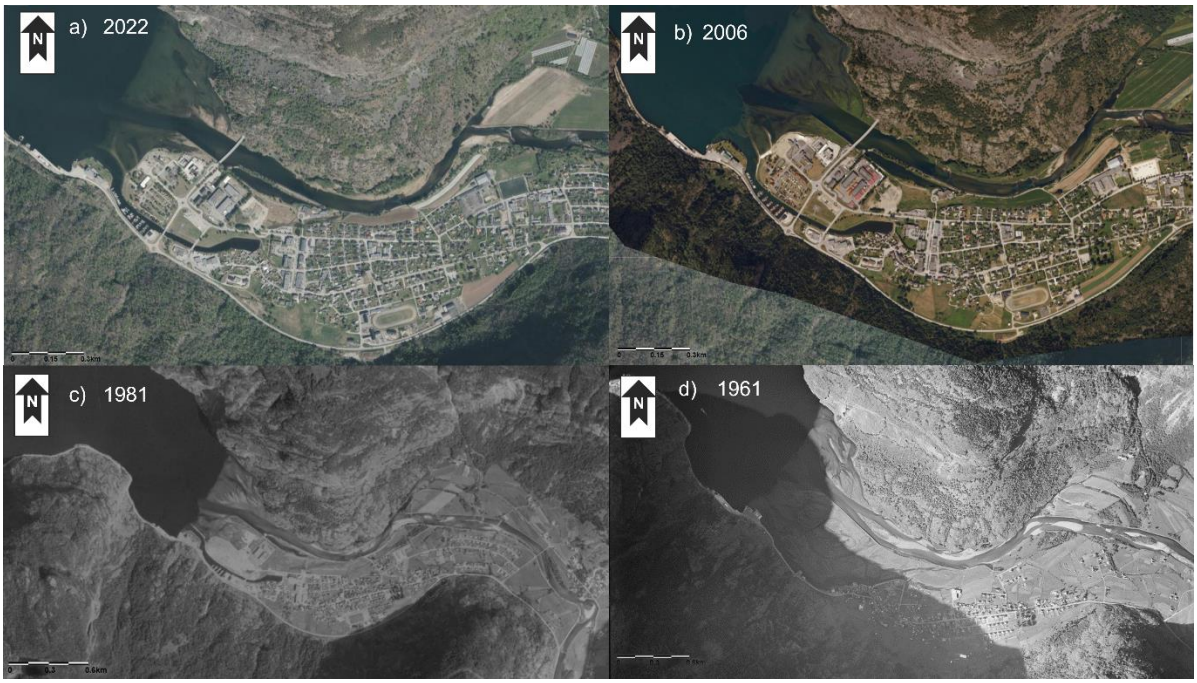

Figure 10, Satellite image of the delta in Lærdal in (a) 2022, (b) 2006, (c) 1981 (modified after norgeibilder.no) and (d) 1961 (odified after Statens kartverk (1961) WF-2223-L19.I)

3.5.6 Precipitation of the last 100 years

During the last 100 years, precipitation in the annual mean precipitation in Lærdal increased (Figure 11, red trendline, Norskklimaservicesenter.no).

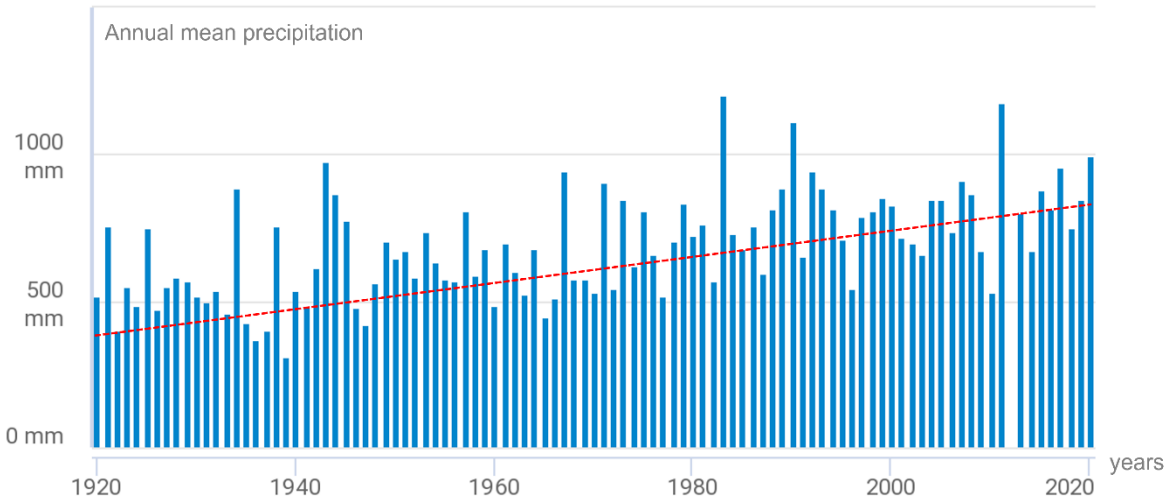

Figure 11, Annual mean precipitation from the measuring station in Maristova, Lærdal from 1920 to 2020. The red dashed line resembles the trendline, indicating a positive trend of increasing precipitation (modified after Norskklimaservicesenter.no).

3.6 Geochemical Background and Dating

3.6.1 Magnetic susceptibility

Magnetic susceptibility is often used in combination with X-ray fluorescence to support and verify interpretations. An example is formed by the relationship between iron and magnetic susceptibility. Both elements tend to correlate very well as magnetic susceptibility usually results out of the magnetite mineral part in iron (Kuhlamnn et al., 2004). For example, this relationship was used for age model transfers of sediment cores (Kuhlmann et al., 2004). The corelation between iron and magnetic susceptibility has also been used to determine sources of sediment origin and identify changes in sediment origin (Møller et al., 2006).

3.6.2 Xray-fluorescence

X-ray fluorescence allows the scan of sediment samples for various elements of the periodic table. It provides the distribution of element occurrences which can be interpreted according to their environmental proxies. These proxies come with a wide variety of interpretations and can help to reconstruct environmental change and climate change (Croudace et al., 2006, Rothwell et al., 2015).

Bromine is commonly used to analyse variations in marine organic matter. It allows to draw conclusions about primary production and oxic or anoxic conditions within the water body of a fjord or lake (Møller et al., 2006, Seki et al., 2019).

It is also possible to investigate changes in the mineral matter composition by using elements such as titantium and iron. Rebolledo et al. (2008) used the correlation between titanium and iron to investigate terrestrial runoff and changes in precipitation. Like the magnetic susceptibility, the Ti/K ratio can be used to determine variations in grain size character and changes of the sources for sediment input (Rothwell et al., 2015, Miserocchi et al., 2016).

XRF can also give information about the abundance of various pollutants within the sediment. For example, accumulation of arsenic, copper, zinc, manganese, and lead can indicate anthropogenic impact and is most likely to be found in harbour or

agricultural areas as well as nearby dumping sites (Ruiz, 2001, Ahmed et al., 2013, Rodríguez-Germade et al., 2014).

3.6.3 Core Dating

A sediment core analysis from the Inner Lærdalsfjord in 2018 provides information regarding the geochemical (XRF and magnetic susceptibility) composition and sedimentation rate of the Inner Lærdalsfjord (Gjerdingen, 2018).

Furthermore, Gjerdingen (2018) provides an age model for the sediment core, using the ^{137}Cs and ^{210}Pb method and an interpolation to the ^{14}C method for dating the core from the Inner Lærdalsfjord (Figure 12). The sedimentation rates result in approximately 0.26 cm/year between 1860 and 1986 and 0.30 cm/year from 1986 to the 2000's (Figure 12).

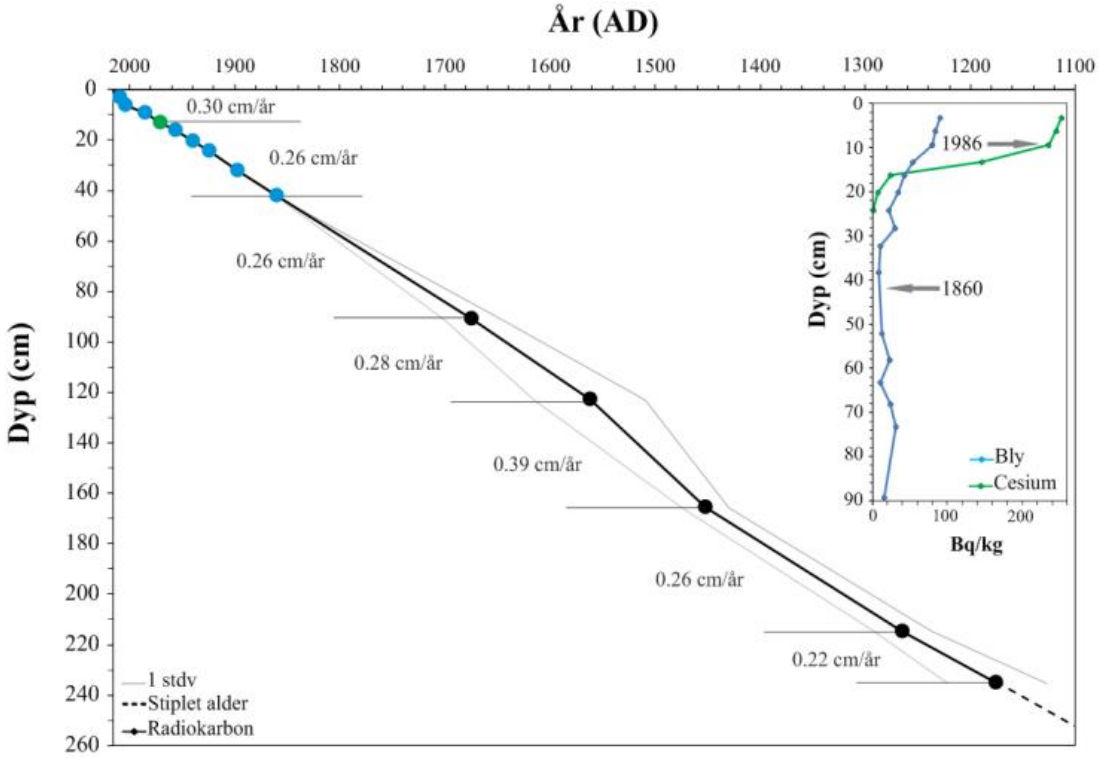

Figure 12, Age model of a sediment core of the Inner Lærdaslfjord, using the ^{137}Cs and ^{210}Pb method, adopted from Gjerdingen (2018)

Additionally, Haflidason (2020) used the same age model from Gjerdingen (2018) to date a parallel core by correlation the gamma density to each other, including an average linear sedimentation rate of 0.22 cm/year for the past 100 years (Figure 13).

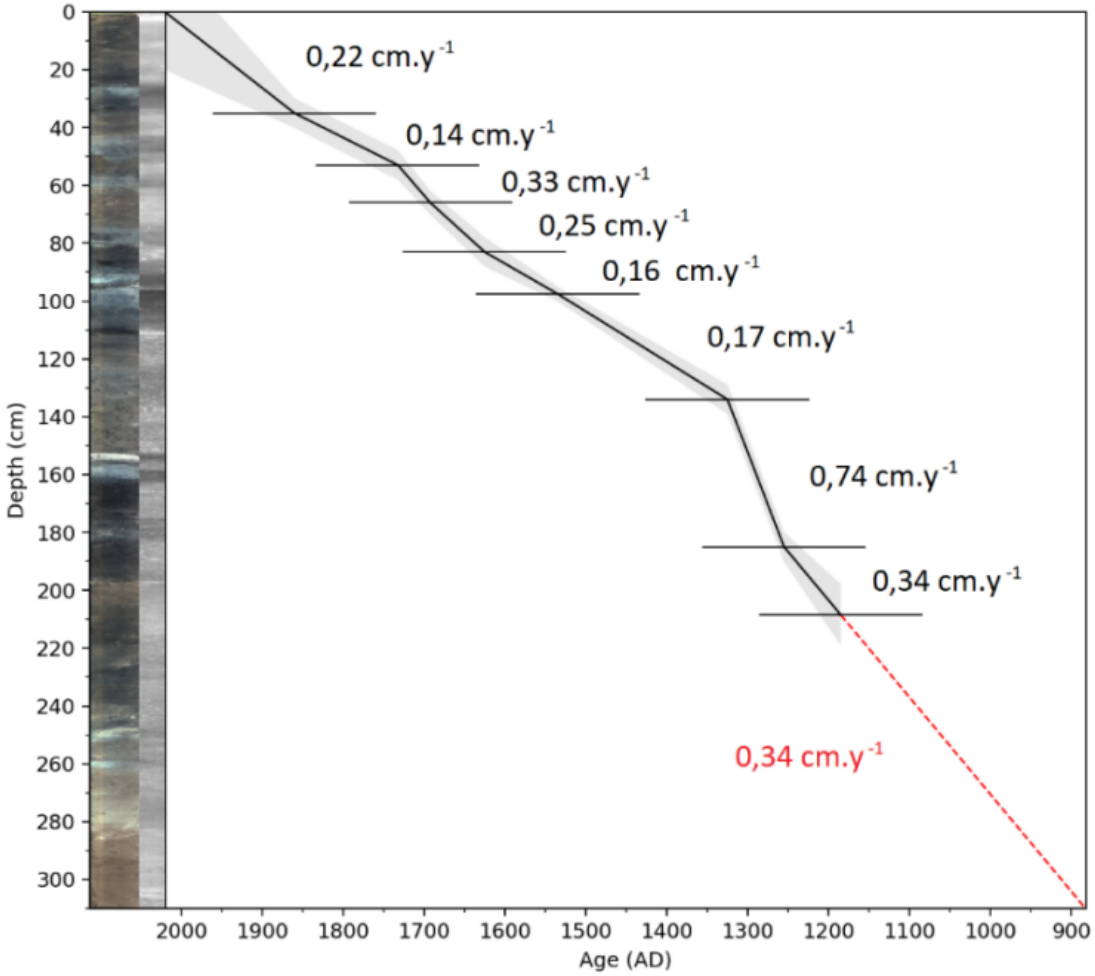

Figure 13, Age model by Haflidason (2020) based on the correlation of the gamma density with a neighbouring sediment core of Gjerdingen (2018) of the Inner Lærdalsfjord.

4. Materials and Methods

4.1 Materials

4.1.1 Sampling Locations

Samples were taken in the Lærdalsfjord on August 30th, 2022 (Figure 14), as part of the *From Mountain to Fjord* program from the Høgskulen på Vestlandet. There are two sediment core samples for each fjord basin and the samples were extracted using a Niemistö (1974) corer. Table 2 contains the sample locations of the cores MF2022-5

(Outer Lærdalsfjord) and MF2022-4 (Inner Lærdalsfjord), as well as the parallel cores of Yang (2023) of the same study, which are being used as reference.

Table 4, Sampling locations of the sediment cores MF2022-4 (Outer Lærdalsfjord), MF2022-5 (Inner Lærdalsfjord) and Yangs (2023) parallel cores MF2022-2 (Inner Lærdalsfjord) and MF2022-3 (Outer Lærdalsfjord).

Core name	Fjord basin	Coordinates	Water depth by extraction	Sediment recovery
MF2022-5	Inner Lærdalsfjord	61°06.506 N 7°26.515 E	55 m	21 cm
MF2022-4	Outer Lærdalsfjord	61°06.530 N 7°25.596 E	110 m	20 cm
MF2022-3	Outer Lærdalsfjord	61°06.226 N 7°25.415 E	123 m	28 cm
MF2022-2	Inner Lærdalsfjord	61°06.288 N 7°27.930 E	52.6 m	23 cm

Figure 14, Sampling locations of sediment cores. The orange dots resemble the location of the cores MF2022-4 and MF2022-5. The red, smaller dots indicate the sampling locations of Yangs (2023) parallel cores MF2022-2 and MF2022-3 (modified after Norgeskart.no).

4.1.2 Core preparation

The sediment cores were cut in half using an automatic saw (Figure 15), since the ITRAX Core scanner for the X-ray fluorescence (XRF) measurements and the Multi-Sensor Core Logger (MSCL) for magnetic susceptibility measurements can scan split sediment cores only.

Figure 15, Setup of a sediment core to be cut open

Afterwards, the open sediment surface was smoothened. For a precise scan it is important to have a surface elevation as even as possible, so the calibrated elevation of the sample is the same throughout the entire core (Croudace et al., 2006).

4.2 Methods

4.2.1 Magnetic susceptibility

The magnetic susceptibility is measured with the GEOTEK Multi-Sensor Core Logger (MSCL-S) located at the Earth Lab of the University of Bergen, Norway. The Multi-Sensor Core Logger scans split cores up to 150 cm length.

The MSCL applies a magnetic field to the sample that any magnetic material within the sample will react to. This magnetism usually applies to mineral matter, while organic matter would be measured as non-magnetic material. The magnetic susceptibility is measured downcore and given in the unit SI*10^{-5} (Kuhlman et al., 2004). Magnetic susceptibility data and XRF data can be combined and together they provide a multifunctional foundation for geochemical analysis on sediments (Kuhlman et al., 2004).

4.2.2 X-ray fluorescence

To determine the elemental distribution within the marine sediment core samples, the sediment cores were scanned with the ITRAX XRF Core Scanner from Cox Analytical Systems (Gothenburg, Sweden) located at the Earth Lab of the University of Bergen, Norway.
The ITRAX Core scanner is a modern and well-established tool in geochemistry to scan sediment cores for various elements between the 3rd and 6th period of the periodic table of elements, in a time saving and non-destructive way (Rothwell et al., 2015), starting at the atomic number of Z=13 (Figure 16).
The ITRAX scan can be performed with using either a 3 kW Mo-tube or a 2.4 kW Cu-tube (Croudace et al. 2006). For the analysis of the Lærdalsfjord samples, a Mo-tube (molybdenum-tube) has been used.

The split sediment cores were scanned for 31 elements positioned between Aluminium (Al) and Lead (Pb) in the periodic table of elements (Figure 16).

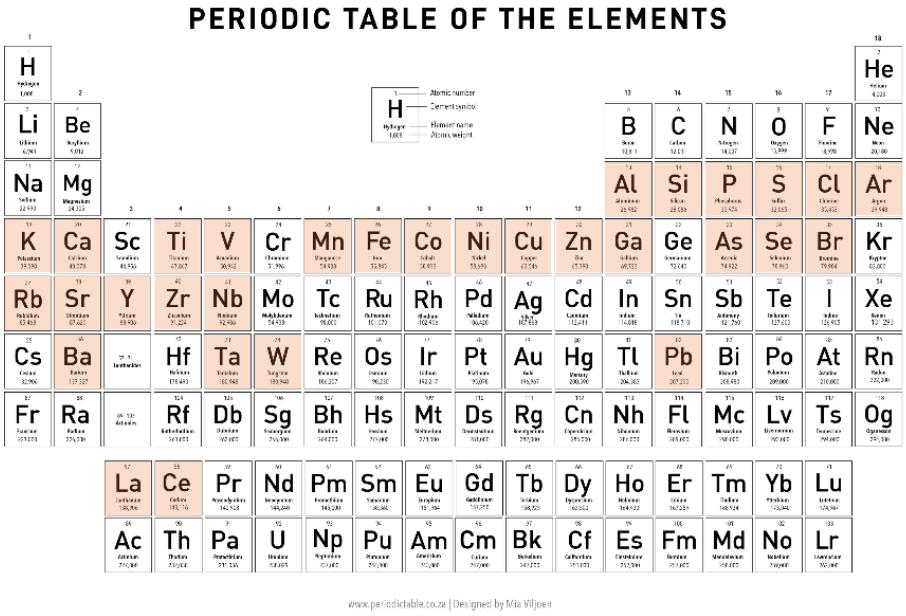

Figure 16, All 31 elements (highlighted) that are scanned with the ITRAX Core Scanner using a Mo-tube (Rothwell et al., 2015) (Figure modified after periodictable.co.za).

The XRF ITRAX scan allows a resemblance of elements measured continuously downcore every 0,05 cm in counts per second (cps). The maximum core length is limited to 180 cm (Croudace et al., 2006). Measurements provide absolute occurrences of the selected elements, though not absolute amounts or concentrations (Croudace et al., 2006). The XRF stack result data is being adjusted using an excel sheet. Measurement rows with values of zero have been taken out for all 31 elements.

Additionally, the ITRAX scan does provide a radiographic image of the core sample (Figure 17, 18).

4.2.2.1 Statistical correlation

To evaluate the relationship between the 31 elements, a statistical approach was made. Howarth et al. (1983) suggested a correlation coefficient of r = 0.44 to determine correlating elements in geochemistry. Thus, elements with a correlation coefficient of r = 0.44 or higher were used (Appendix 4, 5, highlighted elements).

4.2.3 Core Dating

To date the sediment core of the Inner Lærdalsfjord, a correlation to a parallel core by Yang (2023) is being used. Yang (2023) used the method of Paetzel & Dale (2010) by relating freshwater diatom peaks to precipitation peaks of the area. In addition, the earlier estimated sedimentation rates of 0,22 to 0.33 cm/year (Figure 12 Gjerdingen, 2018; Figure 13 Haflidason, 2020) were used for a verification of the resulting time horizons in the sediment cores.

For the correlation with the parallel sediment core of Yang (2023), the elemental bromine measurements from the XRF analysis of the Inner Lærdalsfjord sediment core are compared to the relative abundance of freshwater diatoms in the parallel core of Yang (2023). Bromine in marine sediments indicates the level of marine primary productivity. Thus, as the transport of freshwater diatom concentration increases with increasing precipitation (Paetzel and Dale, 20210; Yang, 2023), a parallel decrease in the marine productivity record and thus in the bromine concentration could be expected (Møller et al., 2006, Ren et al., 2009). Peaks in the relative abundance of freshwater diatoms of the neighbouring core by Yang (2023) should then correlate to lows in bromine, and a dating based on this relationship could be conducted.

For the sediment core from the Outer Lærdalsfjord, a core-to-core correlation between the Inner Lærdalsfjord sediment core (MF2022-5) and the Outer Lærdalsfjord sediments core (MF2022-4) is performed using the respective bromine measurements.

5. Results

5.1 Core description

The core from the Inner Lærdalsfjord (MF2022-5; Figure 17) has a total length of 21 cm. The sediment texture is being categorised as sandy silty clay throughout the whole core. The sediment sample has a salty smell, and no anoxic smell was detected. Several layers are visible throughout the core. The lower parts show black layering. Gravel material was found at a sediment depth of 8 cm, which also is continuously distributed from 21 to 10 cm. There is a shell at 19.5 cm sediment depth.

The colour of the sediment has been determined according to Munsell's Soil Colour Chart (Munsell.com). The sediment colour from 21 to 2 cm has been categorized as very dark grey (2.5Y3/1). The core sample includes a lens formation on one side between 10.5 and 7 cm with a slightly lighter colour (5Y3/2, dark olive grey) for the lens (Figure 17). The sediment colour from the top 2 to 0 cm is dark olive grey (5Y3/2).

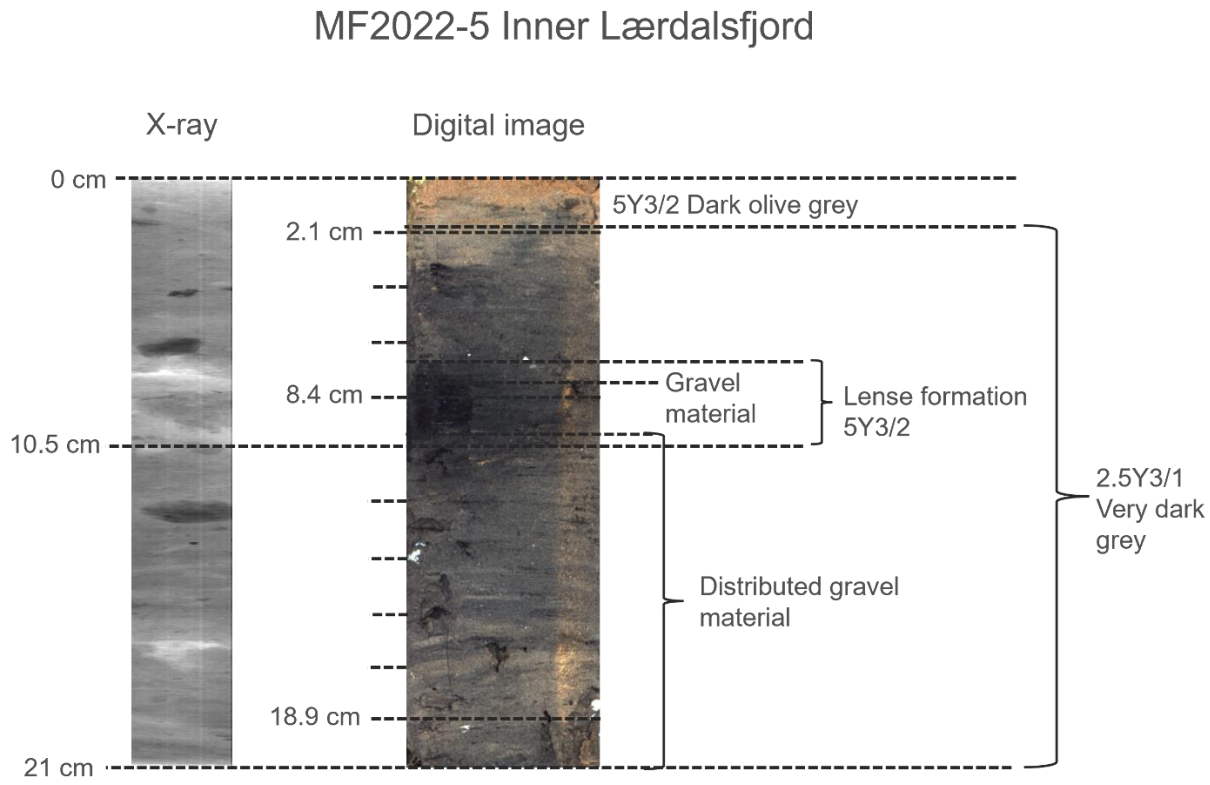

Figure 17, Digital image (right) of sediment core MF2022-5 from the Inner Lærdalsfjord including an X-ray image (left).

The core from the Outer Lærdalsfjord (MF2022-4; Figure 18) has a total length of 20.5 cm. This core is homogenous and does not show any signs of visible layering or coarse material. The entire core has a sandy silty clay texture, and the colour is black (5Y2.5/2) throughout the entire core.

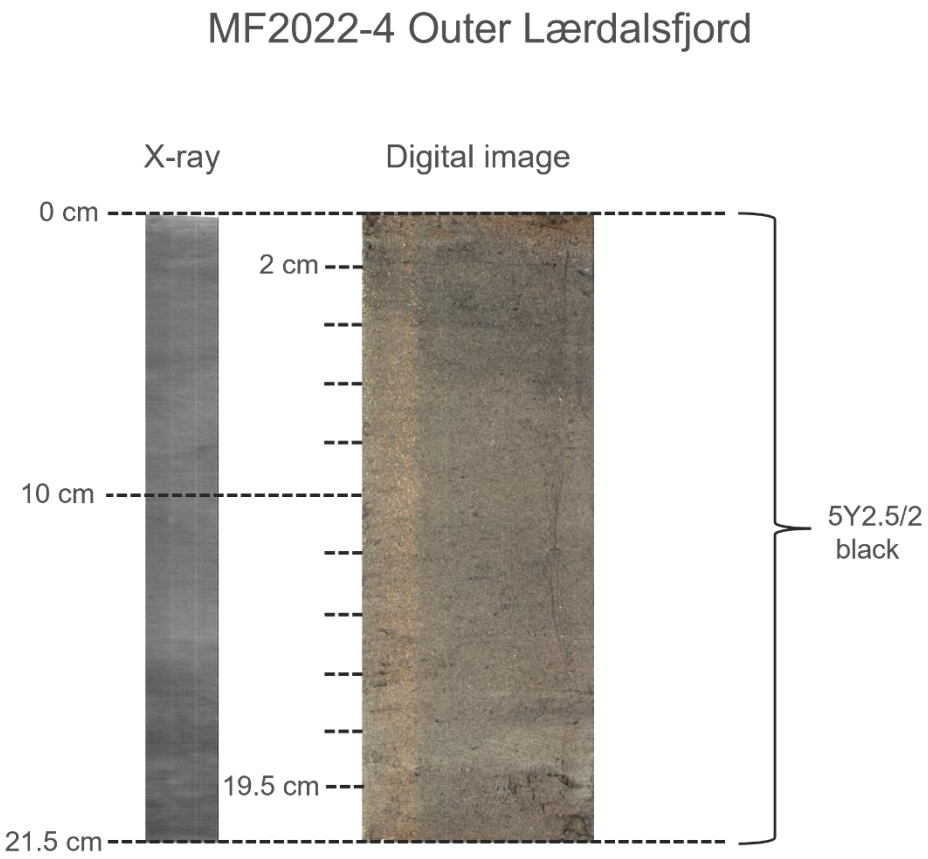

Figure 18, Digital image (right) of sediment core MF2022-4 from the Outer Lærdalsfjord including an X-ray image (left).

5.2 Core Dating

For the dating, an inverted graph of the bromine occurences is being used, as the normalised inverted bromine shows great resemblance in its pattern with the abundance of freshwater diatoms. Thus, it minimizes the sources of error as the normalised inversion of bromine allowed a peak to peak correlation instead of corelating a peak to a low (Figure 19).

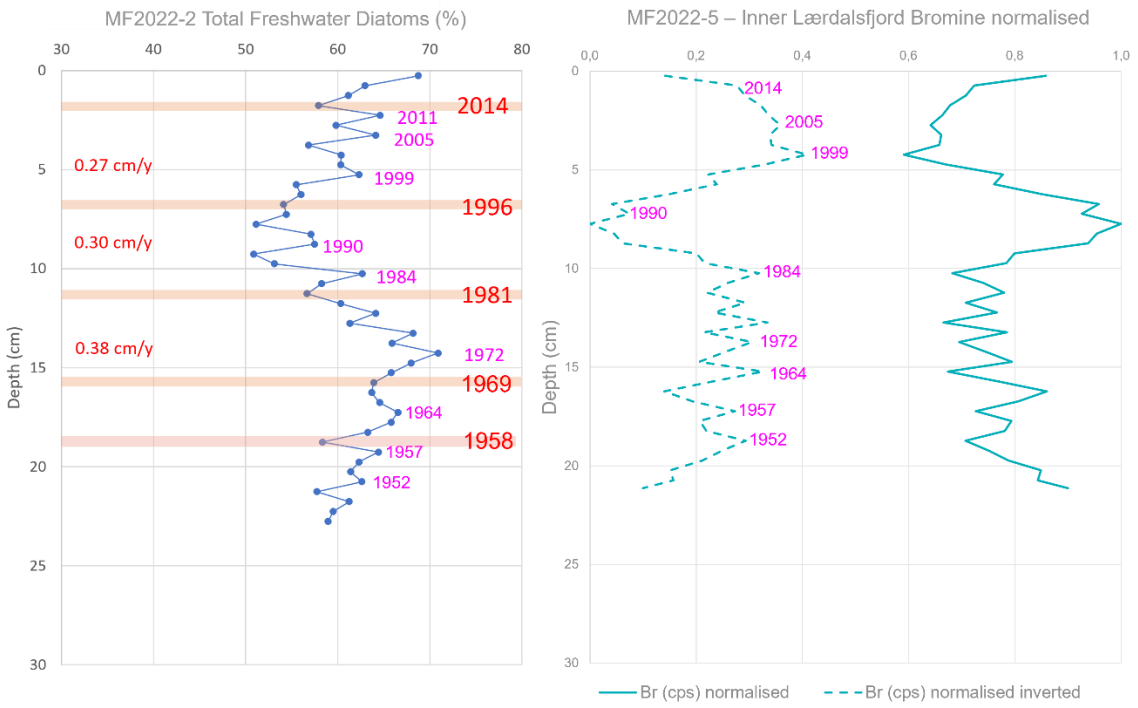

Figure 19, Correlating the dating by Freshwater Diatoms from the parallel core MF2022-2 (left) of Yang (2023) from the Inner Lærdalsfjord to normalised bromine values (right) of core MF2022-5 from the Inner Lærdalsfjord of this thesis.

For the normalisation, the number one is assigned to the highest bromine value in counts per second (cps). Every other value forms its respective fraction of that highest number one.

The inversion is caluclated by subtracting the normalised values from the value one (Equation 1).

Equation 1, Formular to calculate the normalised inverted bromine.

$$Normalised\ inverted\ bromine = 1 - normalised\ bromine$$

The inverted graph from the bromine values from the Inner Lærdalsfjord show significant similarities to the Freshwater diatom abundances. The paralell core of Yang (2023) is slightly longer than the core used for this thesis, thus a manually transfer of the dates based on visual similarities of the peaks was necessary.

Starting with the most significant part of the curve from the inverted bromine graph, the 1990 lowest peaks at 9 cm sediment depth from Yangs core dating were transferred to the lowest peaks at approximately 7 cm sediment depth of the MF2022-5 core. From that point on, the other years were transferred, counting the respective peaks upwards and downwards. This results in the most recent year 2014 estimated to be located approximatley at the first centimeter of the sediment core and 1952 as the oldest year at approximately 18 cm depth.

Based on this dating, the events from the historical background (Phases I to IV of Table 1) were assigned to their respective period of time (Figure 20, red bars). From now on, these events are being refered to as

Phase I: Garbage dumping (1950-1976), refering to the garbage dumping and burning at Raudberg,

Phase II: Hydropower (1974-1988), containing the construction of the two hydropower plants at Borgund (1974) and Stuvane (1988),

Phase III: Tunnel building (1993-1999), covering the period of the construction of the Fodnestunnel and Lærdalstunnel, and

Phase IV: Delta construction (1993 - 2008), resembling the main period of the loss of the natural delta with its highest activity concentrating between 1993 and 2000.

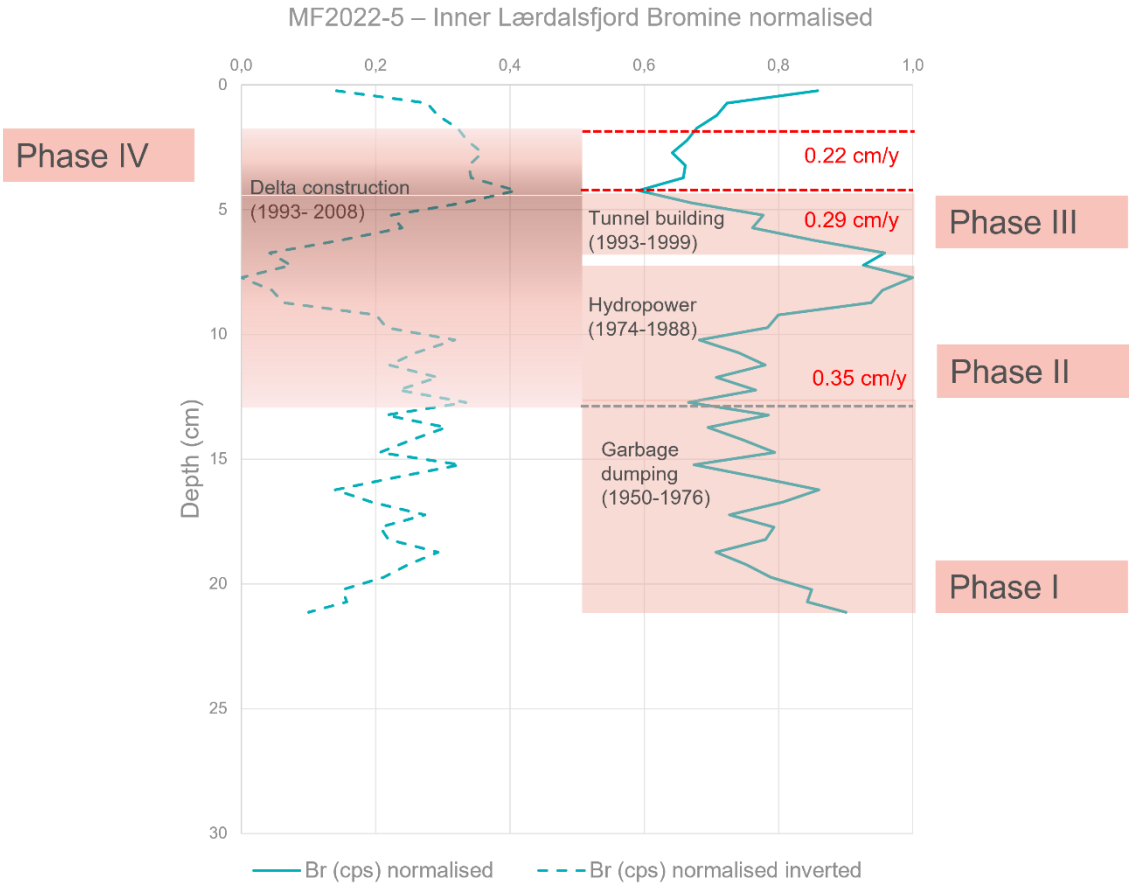

Figure 20, Core dating of the core MF2022-5 from the Inner Lærdalsfjord with respective Phases I to III (right) and Phase IV (left) and sedimentation rates for the Inner Lærdalsfjord. The beginning of Phase II is indicated by the grey dashed line. Phase IV is overlapping with Phase II and Phase III and is depicted separately (left). The increasing colour resembles the increasing construction activity and thus the increasing loss of the natural delta. The colour fades out during less active construction period.

As the *Phase IV Delta construction (1993 - 2008)* started during the mid 1970s and the main activity overlaps with *Phase III Tunnel building (1993-1999), Phase IV Delta construction (1993 - 2008)* is depicted separately on the left side. The colours are getting darker towards the main construction activity from 1993 to 2000 and is fading out before and afterwards, as the exact starting and end point of *Phase IV Delta construction (1993 - 2008)* is unknown.

For further verification of the age model transfer, the sedimentation rates were estimated and compared to the sedimentation rates of Yang (2023) using Equation 2:

Equation 2, Formular for estimating sedimentation rates

$$sedimentation\ rate\ \left[\frac{cm}{y}\right] = \frac{\Delta depth\ [cm]}{\Delta years\ [y]}$$

Since not all of data points that Yang (2023) used for the calculation of the sediment rates can be found clearly in the bromine graph of MF2022-5, the timespans for the estimated sedimentation rates were adjusted. For the calculation, the sedimentation rates were calculated for the *Phases II* to *IV*, as the exact years are known for each Phase. There is no sedimentation rate for *Phase I Garbage dumping (1950 to 1974)*, as the years of the lower part of the sediment core are rather vague and an exact time at the very bottom is unknown. As a result, calculations would be imprecise and thus of lesser value.

Sedimentation rates result in 0.35 cm/y for *Phase II Hydropower (1974 to 1988)* and 0.29 cm/y for *Phase III Tunnel building (1993 to 1999)*.

As the overall *Phase IV Delta construction (1993 to 2008)* started somewhere in the mid 1970s, *Phase IV Delta construction (1993 to 2008)* is depicted seperately on the left (Figure 20) for its overall timespan from mid 1970s to 2008. However, the focus lays on the period from 1993 to 2008, as the main activity happened within this timespan. Because it overlaps with the *Phase III Tunnel building (1993-1999),* the sedimentation rate is calculted from the end of *Phase III Tunnel building (1993-1999)* until 2008 (the end of *Phase IV Delta construction (1993 to 2008)* and equals 0.22 cm/yr (Figure 20, red dashed line).

Comparing these sedimentation rates to Yangs calculation of sedimentation rates of 0.38 cm/y, 0.30 cm/y and 0.27 cm/y (Figure 19) the derivation within the sedimentation rates of the parallel core used for this thesis can be explained by the slightly different timespan used for the calculation. However, the sedimentation rates of both cores are similar which suggests a successfull core-to-core corelation and core dating.

To date the sediment core of the Outer Lærdalsfjord, a core-to-core corelation between MF2022-4 (Outer Lærdalsfjord) and MF2022-5 (Inner Lærdalsfjord) was performed. The bromine graph from the pre-dated Inner Lærdalsfjord was correlated to the bromine graph from the Outer Lærdaslfjord, as both graphs showed an extraordinary resemblence.

However, instead of transferring the different years to matching peaks in the graph, a transfer of the four phases was performed instead. Based on similiarities in overall increases and decreases of the bromine, the respective phases got transferred to the sediment core of the Outer Lærdalsfjord. Sedimentation rates were estimated equally as described above using Equation 2, using the exact same timespans as for the Inner Lærdalsfjord (Figure 21).

Sedimentation rates result in 0.36 cm/y for the period of 1974 to 1988, 0.33 cm/y for the period of 1993 to 1999 and 0.20 cm/y for the period of 1999 to 2014 (Figure 21) for the Outer Lærdalsfjord. Yang (2023) calculated sedimentation rates for the paralell core MF2022-3 from the Outer Lærdalsfjord as well. However, the time intervalls differ considerably from the four Phases used for this estimation. Thus a comparison is possible but not usefull. Nevertheless, Yangs sedimentation rates range from 0.27 cm/y to 0.31 cm/y between different intervals from 1969 to the very top at around 2024.

In addition, the sedimentation rates of both sediment cores (MF2022-4 Outer Lærdalsfjord and MF2022-5 Inner Lærdalsfjord) decrease towards the sediment surface.

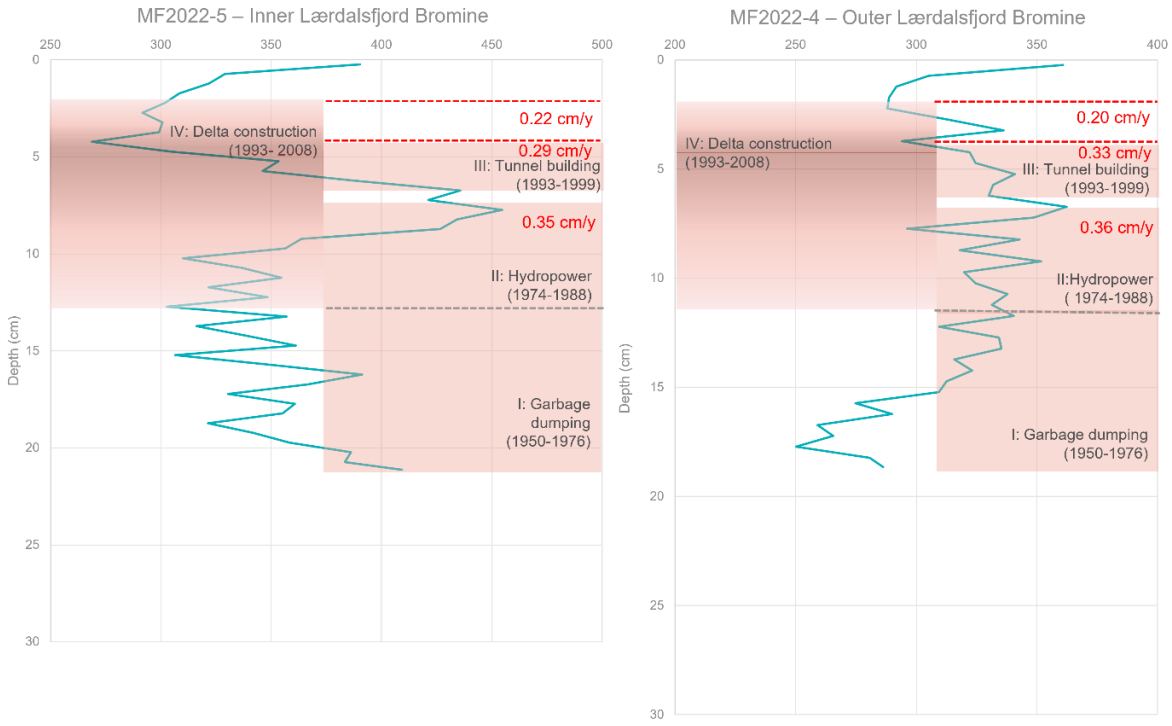

Figure 21, Core dating of the core MF2022-4 (right) from the Outer Lærdalsfjord using a core-to-core corelation from the core MF2022-5 from the Inner Lærdalsfjord (left). The respective Phases I to III (right) and Phase IV (left) and sedimentation rates for the Outer Lærdalsfjord are included. The beginning of Phase II is indicated by the grey dashed line. Phase IV is overlapping with Phase II and Phase III and is depicted separately (left). The increasingly deeper colour resembles the increasing construction activity and thus the increasing loss of the natural delta. The colour fades out during the less active construction period.

There are potential sources of error by dating sediment cores in the way described above. The core-to-core correlation dating from parallel reference cores is not absolute (which would be the case when using for example radiometric dating metods). Furthermore, the age-model transfer by core-to-core corellation is an approximation

only. This means, the estimated years are relative numbers and do represent an aproximated range of the years. Because of that, the Phases I to IV are being refered to for further analysis instead of the corresponding concrete years and no graphs with time-profiles are being created. Additionally, the dating of the very surface of the sediments is uncertain, thus, the youngest years are difficult to include.

5.3 Magnetic Susceptibility

Overall, magnetic susceptibility values for the Inner Lærdalsfjord vary between 0 and 370 Si*10^{-5} (Figure 22).

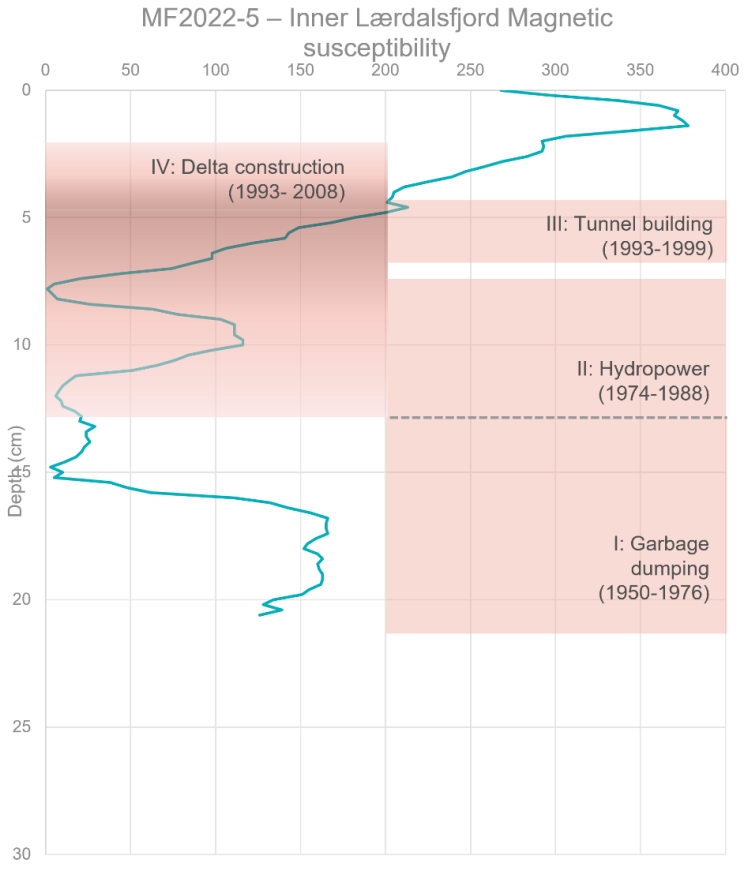

Figure 22, Magnetic susceptibility per depth of the core MF2022-5 from the Inner Lærdalsfjord and the respective Phases I to IV.

Measurements for magnetic susceptibility are elevated during *Phase I Garbage dumping (1950 to 1976)* (Figure 22) and decreasing towards the transition to *Phase II Hydropower (1974-1988)*.

During *Phase II Hydropower (1974-1988)*, magnetic susceptibility is increasing from low values onwards. At the end of this phase, magnetic susceptibility values are close to zero again.

Phase III: Tunnel building (1993-1999) resembles a continuous increase in magnetic susceptibility throughout the entire Phase III, which continues throughout the entire *Phase IV: Delta construction (1993 – 2008).*

The magnetic susceptibility of the Outer Lærdalsfjord has a range between 60 $Si*10^{-5}$ at its lowest and 317 $Si*10^{-5}$ at its highest level (Figure 23). Overall, the magnetic susceptibility of the Outer Lærdalsfjord shows less drastic changes compared to the magnetic susceptibility graph of the Inner Lærdalsfjord. Nevertheless, the magnetic susceptibility values differ for each phase.

Phase I: Garbage dumping (1950-1976) shows a constant increase in magnetic susceptibility, reaching its highest peak of 317 $Si*10^{-5}$ at the end of that phase.

Values are rather constant during *Phase II: Hydropower (1974-1988)* with little variations.

In *Phase III: Tunnel building (1993-1999)*, the magnetic susceptibility values are increasing again, reaching a second peak of 317 $Si*10^{-5}$ right at the beginning of *Phase III: Tunnel building (1993-1999)*.

During the rest of the *Phase III: Tunnel building (1993-1999)*, values are decreasing again until *Phase IV: Delta construction (1993 - 2008)* begins.

With the start of *Phase IV: Delta construction (1993 - 2008)*, magnetic susceptibility values are increasing constantly, reaching the third peak of the highest values of 317 $Si*10^{-5}$ until it is decreasing again.

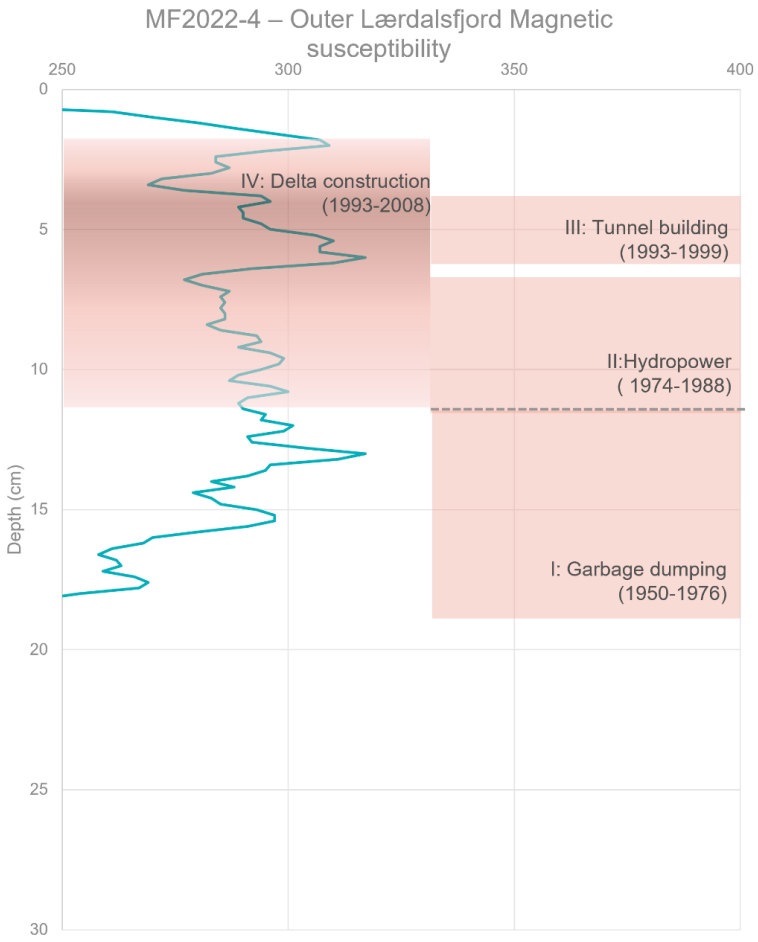

Figure 23, Magnetic susceptibility per depth of the core MF2022-4 from the Outer Lærdalsfjord and their respective Phase I to IV.

5.4 X-ray fluorescence

In this Chapter, the geochemical record is represented. However, not the full range of all 31 elements are being shown here but broken down to a selection of the most varying elements. The selection has been made based on a correlation coefficient greater than r = 0.44 (Howarth et al., 1983) of the sediment core MF2022-5 from the Inner Lærdalsfjord (Appendix 5, red highlighted boxes) for the elements titanium, potassium, iron and manganese and visual distinctive features for the elements lead, copper, niobium and argon. For evaluating and compareing both fjord basins, the same elements were analysed of the sediment core MF2022-4 from the Outer Lærdalsfjord.

5.4.1. Inner Lærdalsfjord Ti/K

The Ti/K ratio of the Inner Lærdalsfjord reaches two out of four maxima during *Phase I: Garbage dumping (1950-1976)* (Figure 24). While starting at lower levels at first, Ti/K values increase during the first quarter of *Phase I: Garbage dumping (1950-1976)*, reaching a maximum ratio of 1.25 cps. Occurrences are decreasing throughout the second and third quarter of *Phase I: Garbage dumping (1950-1976)*, until they are increasing again during the last quarter. *Phase I: Garbage dumping (1950-1976)* ends with the Ti/K ratio reaching its second maximum of a ratio of 1.23 cps (Figure 24).

During *Phase II: Hydropower (1974-1988)*, Ti/K fluctuates between 1.16 cps to 1.23 cps, with an overall increasing trend. However, the maximum of 1.25 cps is reached at the beginning of *Phase III: Tunnel building (1993-1999)* (Figure 24).

Phase III: Tunnel building (1993-1999) shows an overall decrease in the Ti/K ratio, which continues throughout the first half of *Phase IV: Delta construction (1993 - 2008)*. The second half of *Phase IV: Delta construction (1993 - 2008)* is followed by an increase in Ti/K, where it also reaches it forth and last maximum of 1.24 cps (Figure 24).

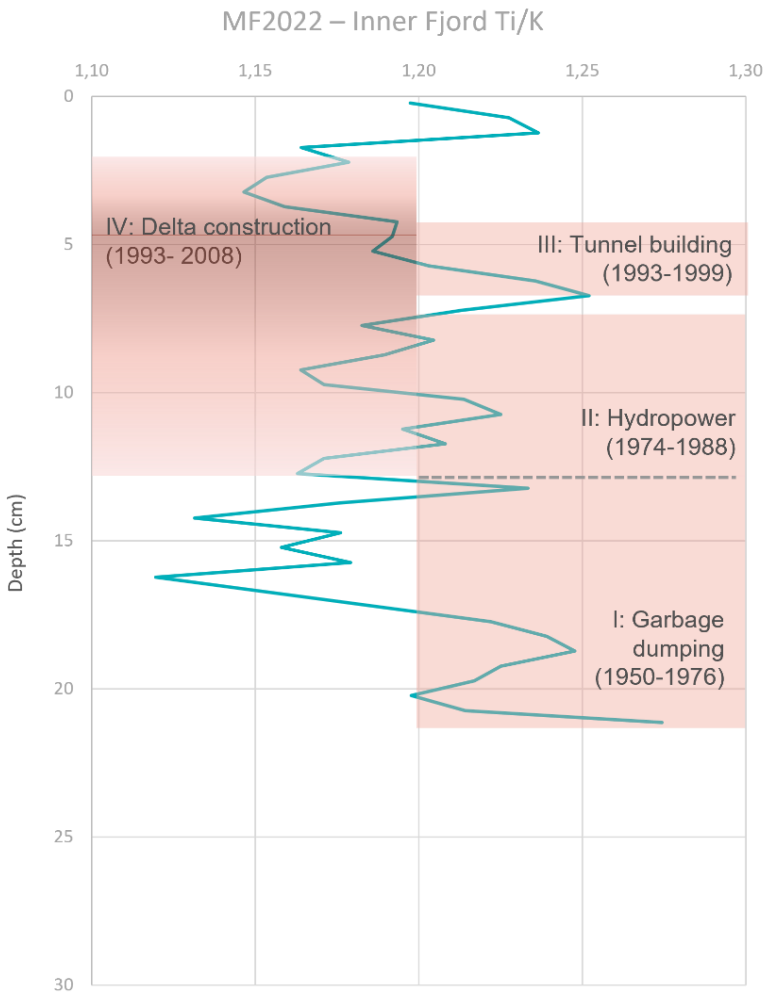

Figure 24, Ti/K ratio per depth of the core MF2022-5 from the Inner Lærdalsfjord and their respective Phase I to IV.

5.4.2 Inner Lærdalsfjord titanium (Ti) and iron (Fe)

Titanium and iron follow each other. Thus, they are described together (Figure 25). During *Phase I: Garbage dumping (1950-1976)*, titanium and iron are increasing. Both reach their overall maximum of 3221 cps (titanium) and 64 443 cps (iron) in the middle of this *Phase I: Garbage dumping (1950-1976)*. At the end of *Phase I: Garbage dumping (1950-1976)*, both elemental occurrences are decreasing again to a total count of 2660 cps for titanium and 57 175 cps for iron (Figure 25).

Phase II: Hydropower (1974-1988) includes a rather constant variation of titanium and iron. However, both elements follow an overall decreasing pattern as titanium decreases from 2660 cps to 2428 cps and iron decreases from 57 175 cps to 54 591 cps (Figure 25).

During the short *Phase III: Tunnel building (1993-1999)*, titanium and iron do not show any significant changes until *Phase IV: Delta construction (1993 - 2008)* starts. With the beginning of this Phase, titanium and iron are increasing again. Both reach their second maximum of 2871 cps (titanium) and 59 756 cps (iron) close to the end of Phase IV (Figure 25).

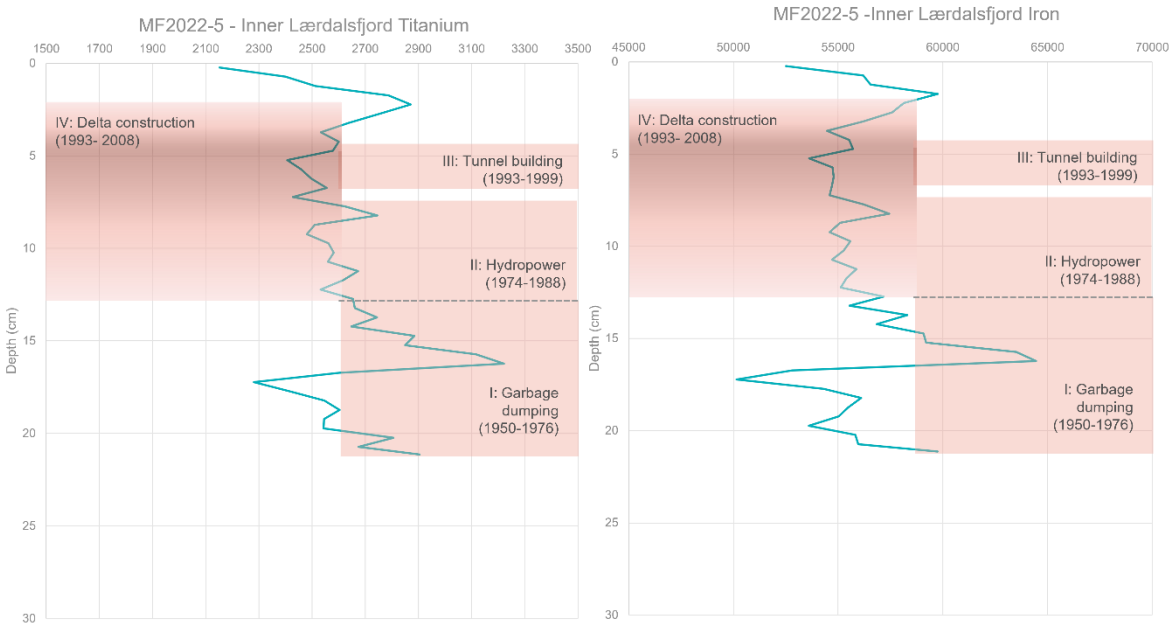

Figure 25, Titanium (left) and iron (right) occurrences per depth of the core MF2022-5 from the Inner Lærdalsfjord and their respective Phase I to IV.

5.4.3 Inner Lærdalsfjord bromine (Br)

Bromine values of the Inner Lærdalsfjord range between 269 counts per seconds (cps) and 455 cps (Figure 26). During *Phase I: Garbage dumping (1950-1976),* the bromine has a decreasing trend (Figure 26), however no significant peaks are detected.

In *Phase II: Hydropower (1974-1988),* bromine fluctuates during the first half of this Phase until it increases throughout the entire second half of *Phase II: Hydropower (1974-1988)*. Furthermore, this *Phase II: Hydropower (1974-1988)* ends with bromine reaching its maximum of 455 cps (Figure 26).

Phase III: Tunnel building (1993-1999) follows with an immediate decrease of bromine counts until it reaches its minimum at 268 cps at the very end of *Phase III: Tunnel building (1993-1999)* (Figure 26).

From the minimum onwards, bromine is increasing again throughout *Phase IV: Delta construction (1993 - 2008)* until 322 cps at the end of the Phase (Figure 26).

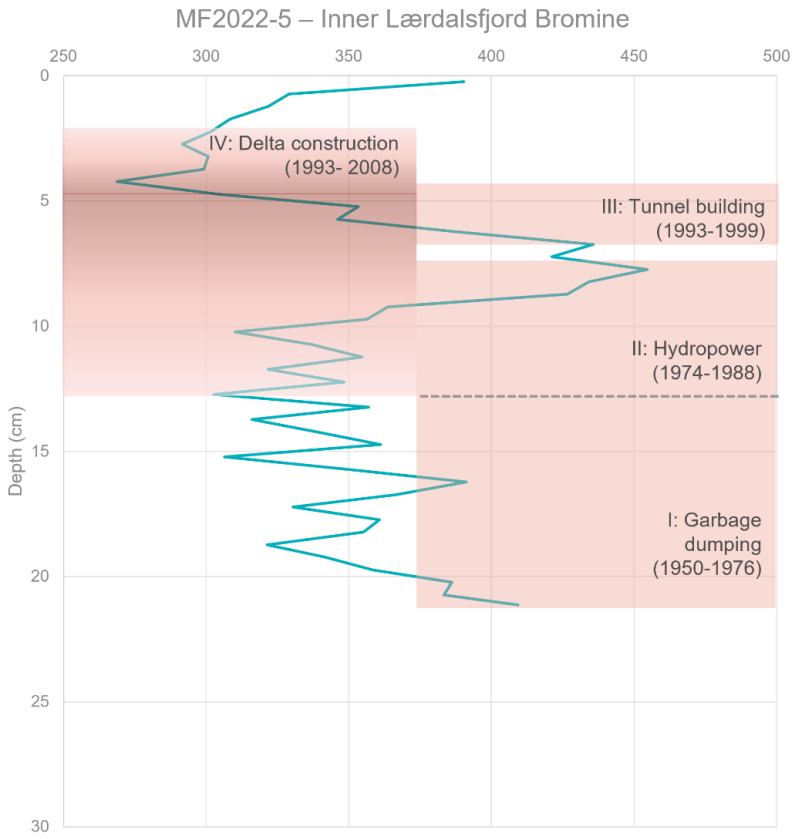

Figure 26, Bromine occurrences per depth of the core MF2022-5 from the Inner Lærdalsfjord and their respective Phase I to IV.

5.4.4 Inner Lærdalsfjord lead (Pb), argon (Ag), copper (Cu) and niobium (Nb)

The occurrences of the metals lead, argon, copper and niobium are being described together as they follow a similar pattern (Figure 27).

During *Phase I: Garbage dumping (1950-1976)*, all four metals are increasing and reaching their respective maximum of 250 cps for lead, 300 cps for argon, 80 cps for copper and 450 cps for niobium (Figure 27). At the end of *Phase I: Garbage dumping (1950-1976)*, lead, copper and niobium are decreasing again. The only exception is formed by argon, which stays at its increased occurrences (Figure 27).

During *Phase II: Hydropower (1974-1988)*, lead, copper and niobium are continuously decreasing while the values for argon stay at their previous increased level (Figure 27).

Phase III: Tunnel building (1993-1999) continues with a decrease of copper and niobium, while lead and argon slightly increase (Figure 27).

The last *Phase IV: Delta construction (1993 - 2008*) follows with a general decrease in all four metals (Figure 27).

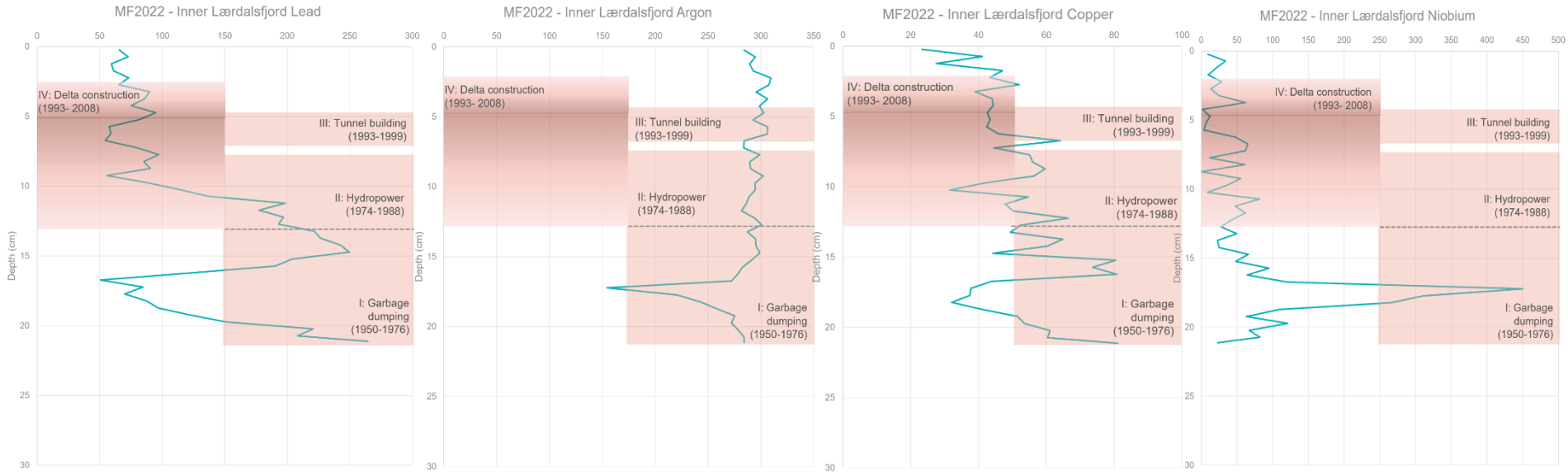

Figure 27, Overview of metal occurrences per depth of the core MF2022-5 from the Inner Lærdalsfjord of lead, argon), copper and niobium.

5.4.5 Inner Lærdalsfjord manganese (Mn)

Manganese occurrences overall range between 500 cps and 710 cps (Figure 28).

During *Phase I: Garbage dumping (1950-1976)*, manganese gradually decreases until it reaches 553 cps at the middle of *Phase I: Garbage dumping (1950-1976)*. Then, values are increasing again until they reach their maximum at 553 cps. Afterwards, manganese occurrences are gradually decreasing again until *Phase II: Hydropower (1974-1988)* starts.

Throughout Phase II, manganese decreases continuously throughout two third of *Phase II: Hydropower (1974-1988)* from 613 cps to 582 cps. Towards the end, manganese occurrences are increasing again to 601 cps.

Phase III: Tunnel building (1993-1999) resembles a gradual increase from 574 cps to 613 cps.

Phase IV: Delta construction (1993 - 2008) shows overall stable manganese levels with little variations between 587 cps and 606 cps.

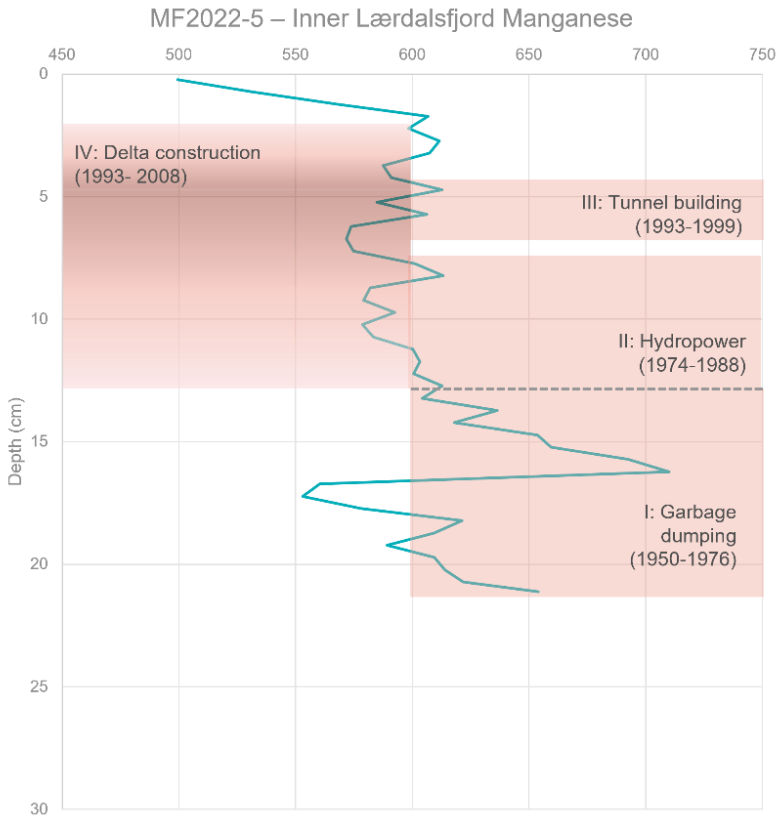

Figure 28, Manganese occurrences per depth of the core MF2022-5 from the Inner Lærdalsfjord and their respective Phase I to IV.

5.4.6 Outer Lærdalsfjord bromine (Br)

In *Phase I: Garbage dumping (1950-1976)* bromine values are increasing constantly, starting at 250 cps until they reach 309 cps and *Phase II: Hydropower (1974-1988*) is about to start (Figure 29).

During *Phase II: Hydropower (1974-1988)*, bromine reaches a steady level with a mean of approximately 350 cps until the end of *Phase II: Hydropower (1974-1988)*, as it decreases to 296 cps and then increases up to 362 cps again. Bromine occurrences reach their maximum of 362 cps at the very end of *Phase II: Hydropower (1974-1988)* (Figure 29).

Phase III: Tunnel building (1993-1999) is resembled by a constant decrease of bromine occurrences from 362 down to 294 cps, which also resembles the second minimum (Figure 29).

Phase IV: Delta construction (1993 - 2008) begins with an increase from 294 cps up to 336 cps, followed by a nearly equal decrease of bromine occurrences from 336 cps to 288 cps during the first half of the phase. Then, bromine occurrences are stagnant until they are increasing again from 288 cps to 305 cps at the end of *Phase IV: Delta construction (1993 - 2008)* (Figure 29).

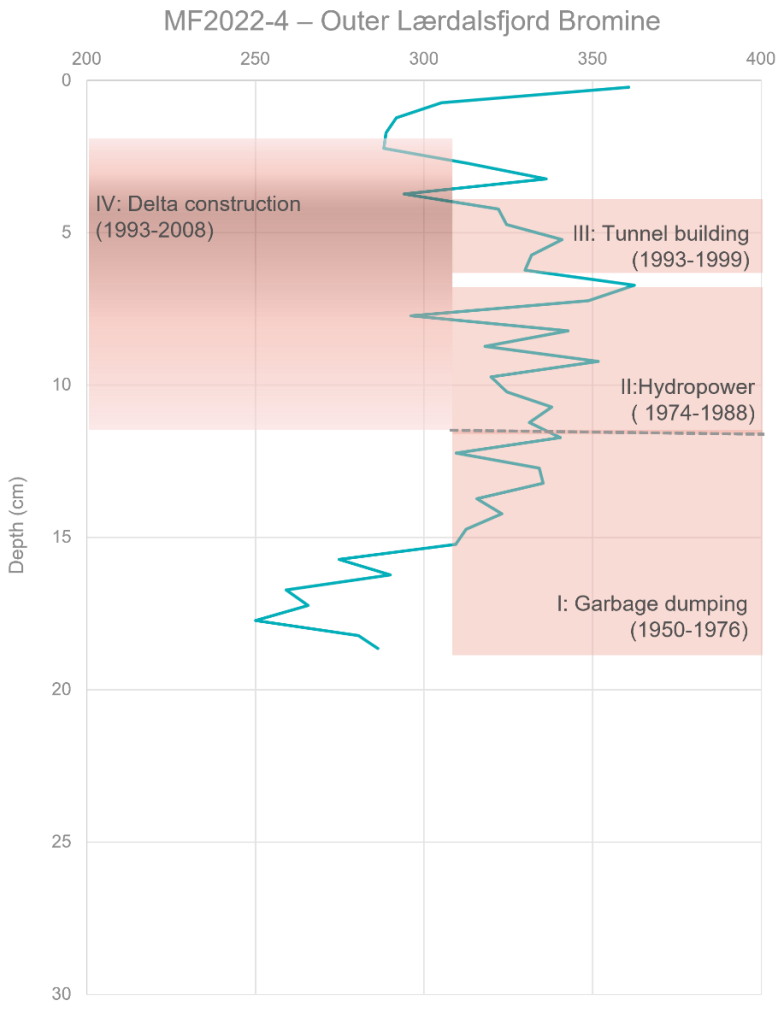

Figure 29 Bromine occurrences per depth of the core MF2022-4 from the Outer Lærdalsfjord and their respective Phase I to IV.

5.4.7 Outer Lærdalsfjord copper (Cu)

The occurrences of copper in the sediment core of the Outer Lærdalsfjord range between 43 cps and 81 cps (Figure 30). Variations are nearly constant throughout all four Phases.

Only *Phase III: Tunnel building (1993-1999)* indicates a slightly decreasing trend from 47 cps down to 42 cps compared to the previous *Phase I: Garbage dumping (1950-1976)* and *Phase II: Hydropower (1974-1988)* where occurrences range around a mean value of approximately 63 cps (Figure 30).
In *Phase IV: Delta construction (1993 - 2008)*, copper occurrences increase again to a mean value of approximately 55 cps (Figure 30).

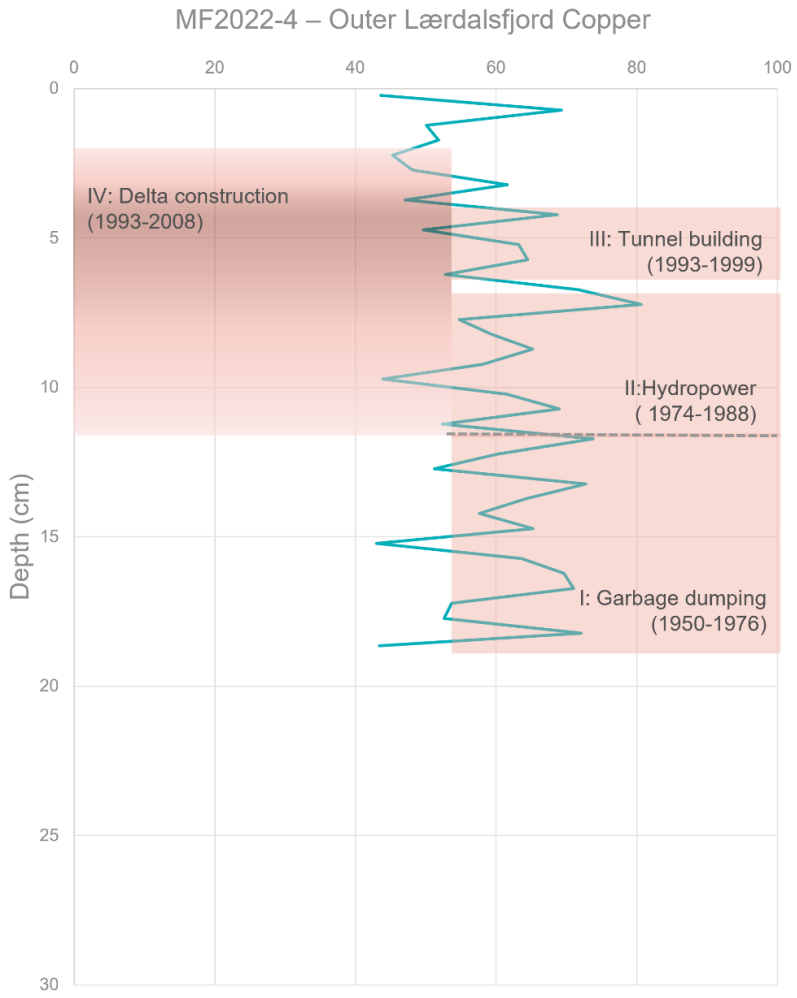

Figure 30, Copper occurrences per depth of the core MF2022-4 from the Outer Lærdalsfjord and their respective Phase I to IV.

5.4.8 Outer Lærdalsfjord manganese (Mn) and iron (Fe)

Manganese and iron correlate (Appendix 5), thus both graphs will be described together.
In general, manganese and occurrences are constant during all four Phases with a slightly decreasing trend (Figure 31).

Both elements are constant throughout the first half of *Phase I: Garbage dumping (1950-1976)*, while they decrease from 714 cps to 622 cps for manganese, and from 60 000 cps to 55 630 cps throughout the second half of *Phase I: Garbage dumping (1950-1976)* (Figure 31).
Phase II: Hydropower (1974-1988) resembles equally constant occurrences of manganese and iron.

In *Phase III: Tunnel building (1993-1999)* manganese decreases from 628 to 627 cps, while iron decreases simultaneously from 54 739 to 53 392 cps (Figure 31).

Manganese ranges between 573 cps and 632 cps during *Phase IV: Delta construction (1993 - 2008)* iron ranges from 49 617 cps to 50 181 cps.

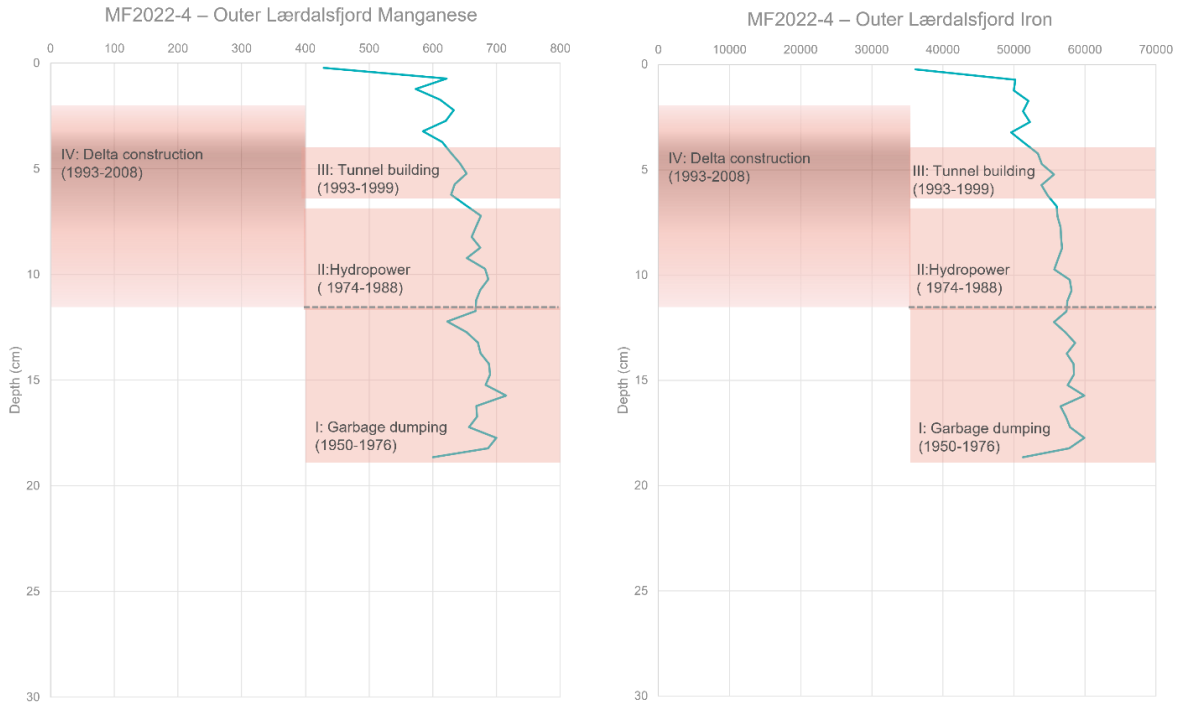

Figure 31, Manganese (left) and iron (right) occurrences per depth of the core MF2022-4 from the Outer Lærdalsfjord and their respective Phase I to IV.

5.4.9 Outer Lærdalsfjord niobium (Nb)

Niobium occurrences are homogenous throughout all four Phases, generally ranging between 0 cps and 70 cps (Figure 32).

During *Phase I: Garbage dumping (1950-1976)* niobium has constant mean values of 50 cps for the upper half of the Phase. At the end of *Phase I: Garbage dumping (1950-1976)*, occurrences decrease until 0 cps (Figure 32).
Niobium reaches maximum occurrences of 30 cps but being at 0 cps most of the time during *Phase II: Hydropower (1974-1988)* (Figure 32).
In *Phase III: Tunnel building (1993-1999)*, niobium reaches its maximum of 70 cps, decreasing back to 0 cps right after (Figure 32).
Phase IV: Delta construction (1993 - 2008) resembles a constant mean occurrence of 2 cps (Figure 32).

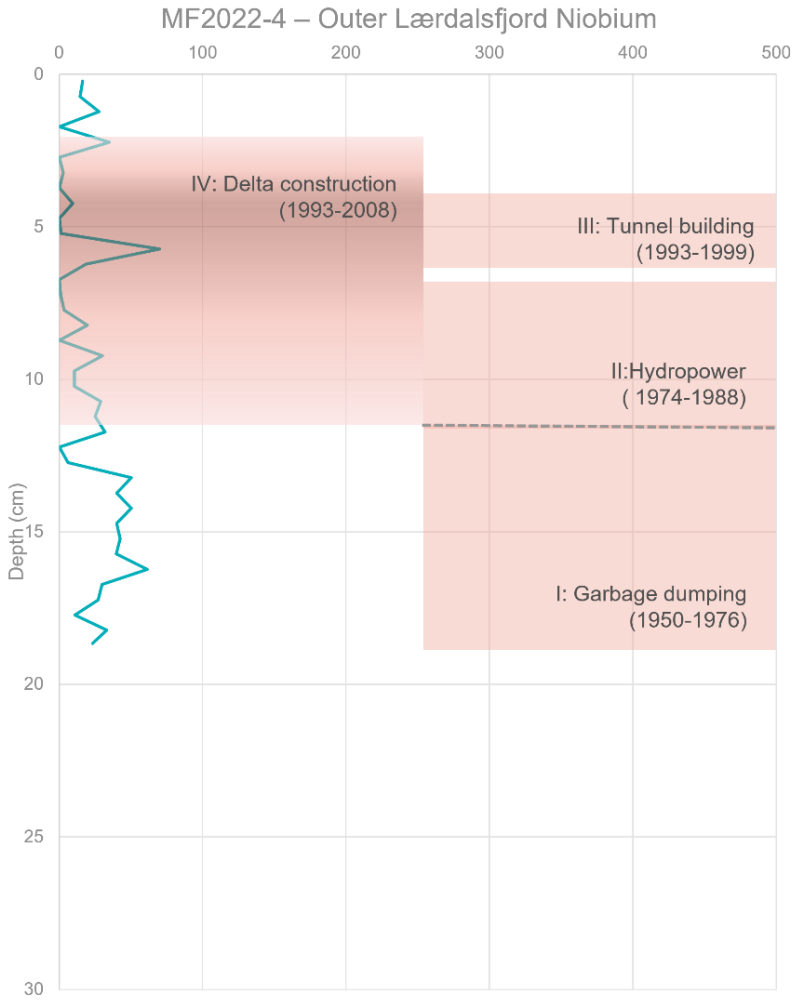

Figure 32, Niobium occurrences per depth of the core MF2022-4 from the Outer Lærdalsfjord and their respective Phase I to IV.

5.4.10 Outer Lærdalsfjord lead (Pb)

Lead occurrences are gradually increasing during *Phase I: Garbage dumping (1950-1976).* Occurrences are overall ranging between 74 cps and 175 cps in *Phase I: Garbage dumping (1950-1976)* (Figure 33).

The gradual increase continuous throughout *Phase II: Hydropower (1974-1988).* Lead reaches its first maximum of 198 cps at the very end of this *Phase II: Hydropower (1974-1988)* (Figure 33).

Phase III: Tunnel building (1993-1999) is resembled by a gradually decrease of lead from 165 cps down to its very minimum of 84 cps, which simultaneously marks the beginning of *Phase IV: Delta construction (1993 - 2008)* (Figure 33).

From the minimum onwards, lead increases constantly throughout *Phase IV: Delta construction (1993 - 2008)* until it reaches its maximum of 272 cps at the very end of the Phase (Figure 33).

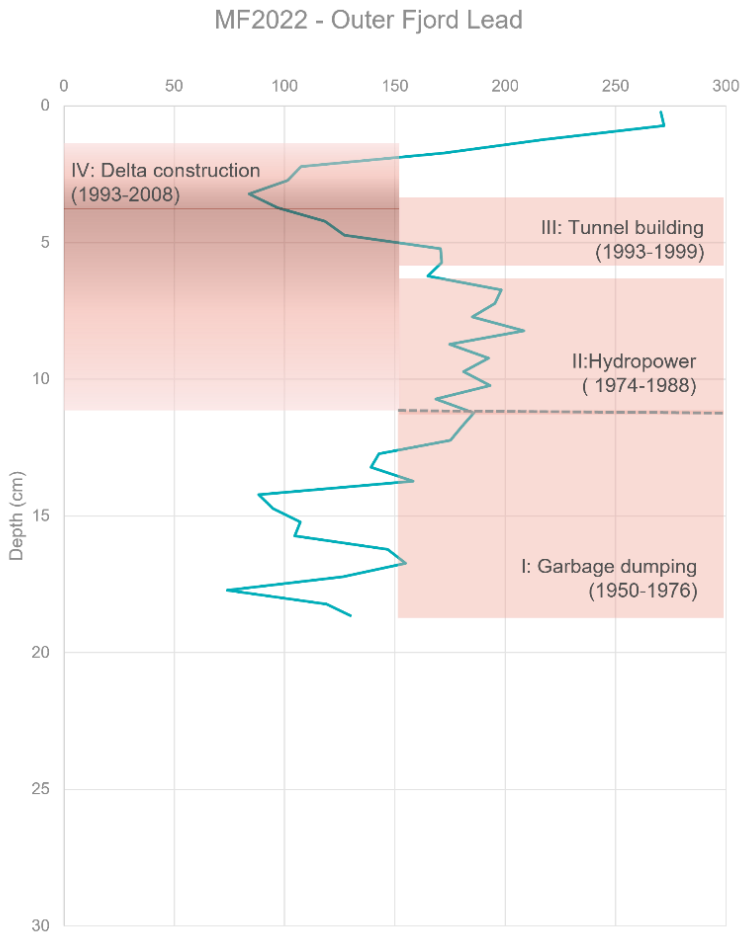

Figure 33, Lead occurrences per depth of the core MF2022-4 from the Outer Lærdalsfjord and their respective Phase I to IV.

6. Discussion

6.1. Environmental significance of the sediment geochemistry in the Inner Lærdalsfjord

In the following, simultaneous changes within different elements are being discussed and linked to their respective causes.

6.1.1 Potassium/titanium ratio (K/Ti ratio) and magnetic susceptibility

Looking at the magnetic susceptibility (blue) signal from the Inner Lærdalsfjord, it is visible that it follows the same pattern as the Ti/K ratio (red) except for the upper 7 cm. Figure 34 shows both signals assembled.

Magnetic susceptibility and Ti/K measurements are from the same sediment core but measured by different devices. Thus, it is possible for both measurements to start at a slightly earlier or delayed point than depicted in the graphs. The exact point of origin is uncertain. As a result, the Graph of the Ti/K ratio can be re-adjusted and be positioned higher as the magnetic susceptibility (Figure 34).

Ti/K is an elemental proxy for variations in grain size character and changes of the sources for sediment input (Miserocchi et al., 2016, Rothwell et al., 2015). As magnetic susceptibility also indicates changes in sediment input and general mineral matter (Møller et al., 2006), the Ti/K ratio and magnetic susceptibility are assumed to change simultaneously.

As the *Phase I: Garbage dumping (1950-1976)* contains the garbage dumping and burning at Raudberg, it is assumed that there were a variety of metal material among the dumping material including some of magnetic content. This results in increased magnetic susceptibility values. Additionally, the Ti/K ratio changes accordingly as it first increases and then decreases with the magnetic susceptibility. Since overall low magnetic susceptibility values indicate the same source of sediment origin (Møller et al., 2006) the decrease from high to low values at the transition from *Phase I* to *Phase II: Hydropower (1974-1988)* can be interpreted as such a change in the sediment origin. Furthermore, this pattern is followed independently by both proxies, the Ti/K ratio and the magnetic susceptibility.

After the transition period between *Phase I: Garbage dumping (1950-1976)* and *Phase II: Hydropower (1974-1988)*, both parameters (magnetic susceptibility and Ti/K) are increasing again. As *Phase II* refers to the hydropower constructions of the two hydropower plants built at Stuvane and Borgund, and a link between these events and the geochemical record can be drawn. Increased Ti/K and magnetic susceptibility indicate a different sediment origin than in *Phase I: Garbage dumping (1950-1976)*. As the hydropower plants impact the river velocity, it will also affect the amount and type of grain sizes of sediment that gets transported into the fjord. Thus, it is possible that the hydropower plants are regulating the river Lærdalselv and thus the sediment input into the Inner Lærdalsfjord.

During *Phase III: Tunnel building (1993-1999)*, magnetic susceptibility and Ti/K are increasing again, indicating another change of sediment origin. This Phase covers the period of the construction of the Fodnestunnel and the Lærdalstunnel. Rock material mainly originating from the construction of the Fodnestunnel got dumped into the Inner Lærdalsfjord (Lærdal municipality, 1991,1995, 2005). The rock material from the Fodnestunnel (Table 3) contains magnetic minerals, and here especially clinopyroxene which is magnetic (Delmonte et al., 2018). This surplus content of magnetic clinopyroxene most likely result in an increase in the magnetic susceptibility once the material got into the fjord environment.

Phase IV: Delta construction (1993 - 2008) forms the only exception in this parallel pattern of magnetic susceptibility and the Ti/K ratio, as the Ti/K ratio decreases while the magnetic susceptibility increases continuously. This continuous increase in magnetic susceptibility can be linked to the construction activity on the delta and thus the loss of the natural delta. Even though the delta was mostly built simultaneously to the Fodnestunnel, the rock material might continuously enter the inner Lærdalsfjord due to wave erosion and outwashing of smaller particles. In addition, rock material of similar composition from the Lærdalstunnel (dumped in Tynjadalen; Figure 1c) might have got eroded into the river Lærdalselv and continuously be transported into the Inner Lærdalsfjord. This combination of similar sources containing magnetic minerals, would then result in a continuous increase in magnetic susceptibility, especially as the amount of annual precipitation, and thus runoff into the river, also increased during that time (Figure 11). Furthermore, the loss of the natural delta will most likely affect the outflow velocity and pathway of the suspended matter of the river Lærdalselv into the Inner Lærdalsfjord, as it does not settle on the delta any longer. This might even enhance the effect of different magnetic mineral material entering the Inner Lærdalsfjord.

However, the Ti/K ratio does not follow the increasing trend of the magnetic susceptibility during *Phase IV: Delta construction (1993 - 2008)*. The difference in the Ti/K signal indicate changes in grain sizes, it is possible that the signal caused by variations of grain sizes is dominating. On the other hand, this would also affect the signal of the magnetic susceptibility. Another possibility would be an increased supply of terrestrial organic matter which would dilute the Ti/K signal but not necessarily have an impact on a simultaneously increasing magnetic mineral input. The exact reason for this anti-correlation remains uncertain.

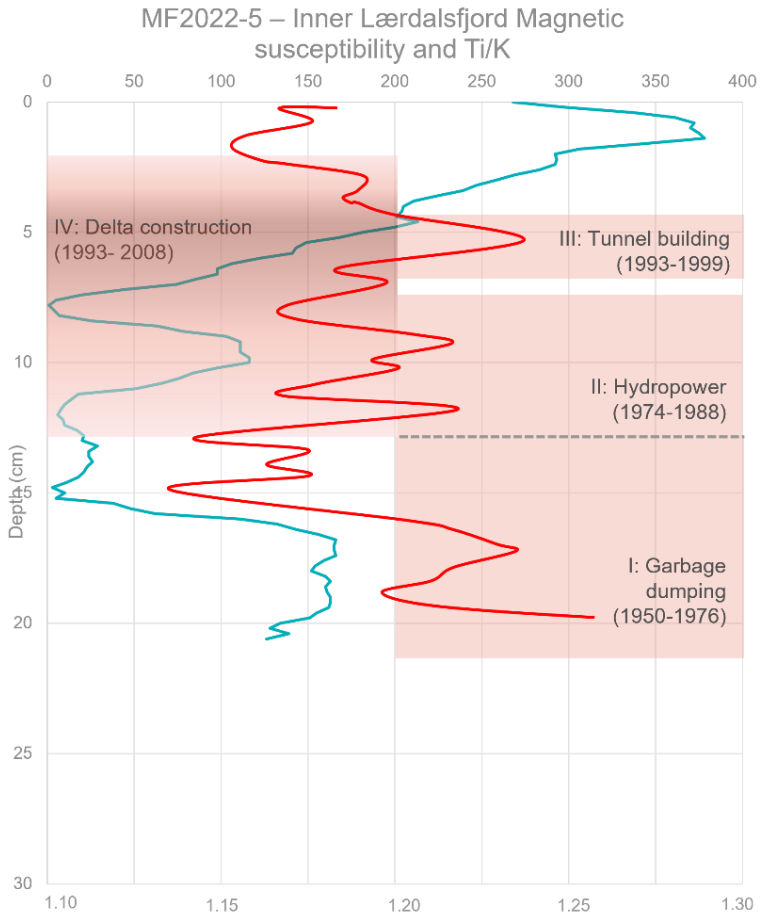

Figure 34, Inner Lærdalsfjord, magnetic susceptibility (blue) on top of Ti/K (red). The upper x-scale resembles the magnetic susceptibility values. The lower x-scale resembles the Ti/K values.

6.1.2 The environmental significance of iron (Fe) and titanium (Ti) in the Inner Lærdalsfjord

Titanium and iron correlate with each other (Kuhlman et al., 2004, Rebolledo et al., 2008, Appendix 5, Figure 25).

The peak in *Phase I: Garbage dumping (1950-1976)* is linked to the garbage dumping and burning in Raudberg. Titanium and iron are common metals used in the metal industry. Thus, they are most likely among the containments that got dumped into the fjord.

In *Phase II: Hydropower (1974-1988)* and *Phase III: Tunnel building (1993-1999)*, iron and titanium gradually decrease. Both elements indicate changes of mineral matter within one source area (Rothwell et al., 2014). Thus, the overall decrease during both phases might indicate gradual changes in the main source area, which is the river Lærdalselv. The source area and the timing of the gradual decrease would imply the initiation and continuation of the hydropower plants as possible cause.

Additionally, the same decrease is visible in the magnetic susceptibility (Figure 22) which indicates generally less mineral input (Møller et al., 2006). As the same timespan within the magnetic susceptibility signal does indicate less mineral input in the sediment, the gradual decrease in iron and titanium might support the interpretation of the hydropower plants affecting the river Lærdalselv and its mineral input.

During *Phase IV: Delta construction (1993 - 2008)*, iron and titanium are increasing again. *Phase IV* is resembling the loss of the natural delta as it got infilled with rock materials from the Fodnestunnel, containing minerals rich in iron and titanium (Table 3). Thus, both signals show the effect of the main activity of the delta infill from 1993 to 2008.

6.1.3 The environmental significance of manganese (Mn) in the Inner Lærdalsfjord

Manganese is an indicator of changes in the magnitude of riverine input (Rothwell et al., 2015).

In *Phase I: Garbage dumping (1950-1976)*, manganese is fluctuating in a wide range (Figure 28). The period between the 1950s and the 1970s is most likely less affected

by anthropogenic impacts into the river Lærdalselv. There are no hydropower plants yet that could possibly temper with the river velocity itself, and no delta infill is affecting the overall outflow of the river Lærdalselv into the fjord, yet. The river Lærdalselv is thus assumed to flow in its natural state and the fluctuations of manganese might not necessarily have their origin in variations in the input of the river Lærdalselv.

Instead, *Phase I: Garbage dumping (1950-1976)* might be linked to the garbage dumping and burning at Raudberg. Manganese increases at the very heart of this period. Manganese is a common element used in the steel industry, as it has an anti-oxidation effect (Coassin et al., 1992). Thus, it is likely to be found among the material that got dumped during this *Phase I*, resulting in a respective increase in manganese in the sediment record.

From *Phase II: Hydropower (1974-1988)* on, manganese fluctuations are reduced gradually. This gradual decrease in the manganese fluctuation is assumed to be governed by the construction of the hydropower plants which were completed in Borgund in 1974 and in Stuvane in 1988. Thus, the gradual decrease of manganese is interpreted as an effect of the hydropower plants that are controlling the river velocity of the river Lærdalselv, leading to an overall less riverine input into the Inner Lærdalsfjord.

During *Phase III: Tunnel building (1993-1999)* and *Phase IV: Delta construction (1993 - 2008)*, manganese fluctuations are gradually increasing again, but keeping its small range. This might be caused by a new equilibrium of the river flow velocity that is reached after that the two hydropower plants are readily constructed. In addition, the annual precipitation increases at the same time (Figure 11) leading to an increase in the river flow velocity and thus an increasing riverine manganese supply into the Inner Lærdalsfjord.

In addition, the tunnel building and the successive rock dumping and delta infill in *Phase IV: Delta construction (1993 - 2008)* will affect the overall outflow of the river Lærdalselv. Thus, the increase of manganese could be interpreted as a general increase in changes in riverine input caused by the rock dumping and the delta infill at the mouth of the river Lærdalselv.

However, the availability of data before *Phase I: Garbage dumping (1950-1976)* would help for the overall interpretation, as it would elaborate whether the fluctuations during this *Phase I* can be interpreted as background concentrations and thus would allow to decide whether the gradual change in manganese concentration in *Phase II: Hydropower (1974-1988)* to *Phase IV: Delta construction (1993 - 2008)* relates to anthropogenic impact or not.

6.1.4 The environmental significance of bromine (Br) in the Inner Lærdalsfjord

Bromine is a proxy for marine organic matter and thus indicates marine productivity (Møller et al., 2006, Ren et al., 2009). During *Phase I: Garbage dumping (1950-1976)*, mean bromine levels are on a stable intermediate level (Figure 36, green arrow). *Phase I: Garbage dumping (1950-1976)* refers to the garbage dumping and burning at Raudberg. The excessive dumping, as well as the ashes from the burning would bring more nutrients into the fjord. Thus, it provides the fjord environment with an increased and diverse supply of nutrients, resulting in an overall stable marine productivity and thus continuously high levels in bromine.

During *Phase II: Hydropower (1974-1988)*, bromine levels are increasing. Simultaneously, the abundance of marine diatoms is increasing as well (Yang, 2023). As the increase in bromine as well as in the diatom abundance is constant throughout the entire establishment of both hydropower plants, it can be concluded that the hydropower plants might have a positive effect on the marine productivity in the Inner Lærdalsfjord by possibly providing enhanced amounts of fine-grained mineral material and thus nutrients.

As *Phase III: Tunnel building (1993-1999)* starts, resembling the entire period of the tunnel constructions and the respective dumping of the rock material into the fjord, bromine is decreasing. For the same period, a decrease of the abundance of the marine diatoms is visible as well (Yang, 2023, and Figure 36, upper green arrow). Generally, dumping of rock material leads to sudden dispersion of sediment. Considering the fact, that the rock dumping occurs over the entire construction period of six years, covering a total amount of over 2 million m^3 (whereof 550 000 m^3 originating from the Fodnestunnel), that got dumped into the fjord, it most likely created constant turbid conditions throughout the entire *Phase III*. Thus, incoming sunlight penetrates less into the water column, resulting in a general decrease in marine productivity due to reduced sunlight and a parallel decrease in diatoms.

In *Phase IV: Delta construction (1993 – 2008)*, bromine is increasing again while the marine diatom abundance continues to decrease (Yang, 2023). The increase in bromine however is surprising. Rock material got continuously dumped into the fjord throughout the delta construction, thus leading to turbid conditions. As a result, bromine values were assumed to stay low. However, they are increasing. A reason for this increase could be the new supply of mineral and terrestrial matter. Additionally, the construction of the delta was most likely to happen more controlled than the overall

rock dumping, thus, turbid conditions could have been generally lower in this *Phase IV:* as they were during the tunnel constructions in *Phase III*.

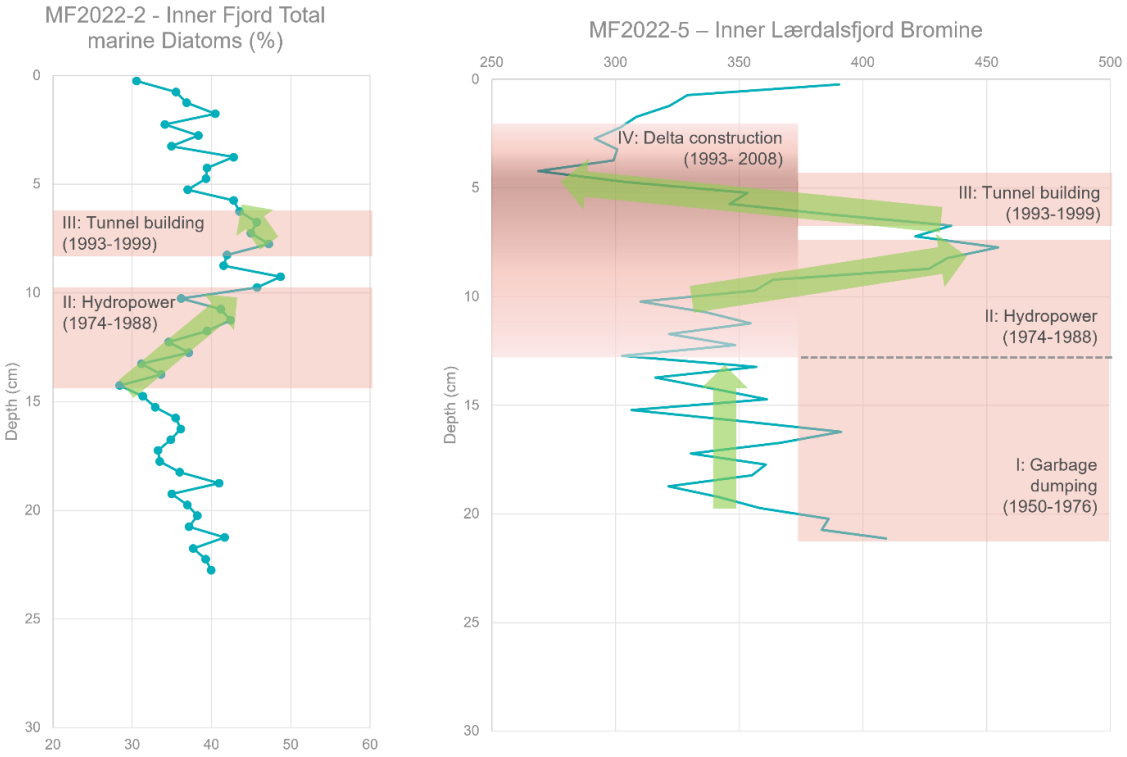

Figure 35, Abundance of total marine diatoms of the Inner Lærdalsfjord (left, modified after Yang 2023) compared to the occurrences of bromine of the Inner Lærdalsfjord (right). The green arrows show changes in the diatom abundances with correlating changes of bromine.

6.1.5 Polluting elements lead (Pb), argon (Ar), copper (Cu), and niobium (Nb) in the Inner Lærdalsfjord

Lead, argon, copper, and niobium do all show a significant peak during *Phase I: Garbage dumping (1950-1976)* (Figure 37). This peak is clearly linked to the garbage dumping and burning at Raudberg. The garbage dumping and burning started in the early 1950s and last until the end of the 1970s. It is assumed, that there was metal material among the dumping material. As metals usually could not be burned. It got instead dumped into the Inner Lærdalsfjord at Raudberg (Leif Hauge 2023, *personal communication*). As a result, the occurrences of these four metals, which are pollutants (Ahmed et al., 2013) are increasingly high during *Phase I*.

As the Klima- og miljødepartementet (1976) established changes in terms of environmental regulations, the effects of increased metal concentrations are limited to *Phase I*.

The metal concentration of lead, copper, and niobium (Figure 37) are continuously decreasing from *Phase II: Hydropower (1974-1988)* until the end of *Phase IV: Delta construction (1993 – 2008)*, supporting the interpretation of the connection between the metal occurrences and garbage dumping and burning at Raudberg. Only Argon stays at a stable level after its peak during *Phase I: Garbage dumping (1950-1976)*. The reasons for these constant increased argon values are puzzling and not elaborated.

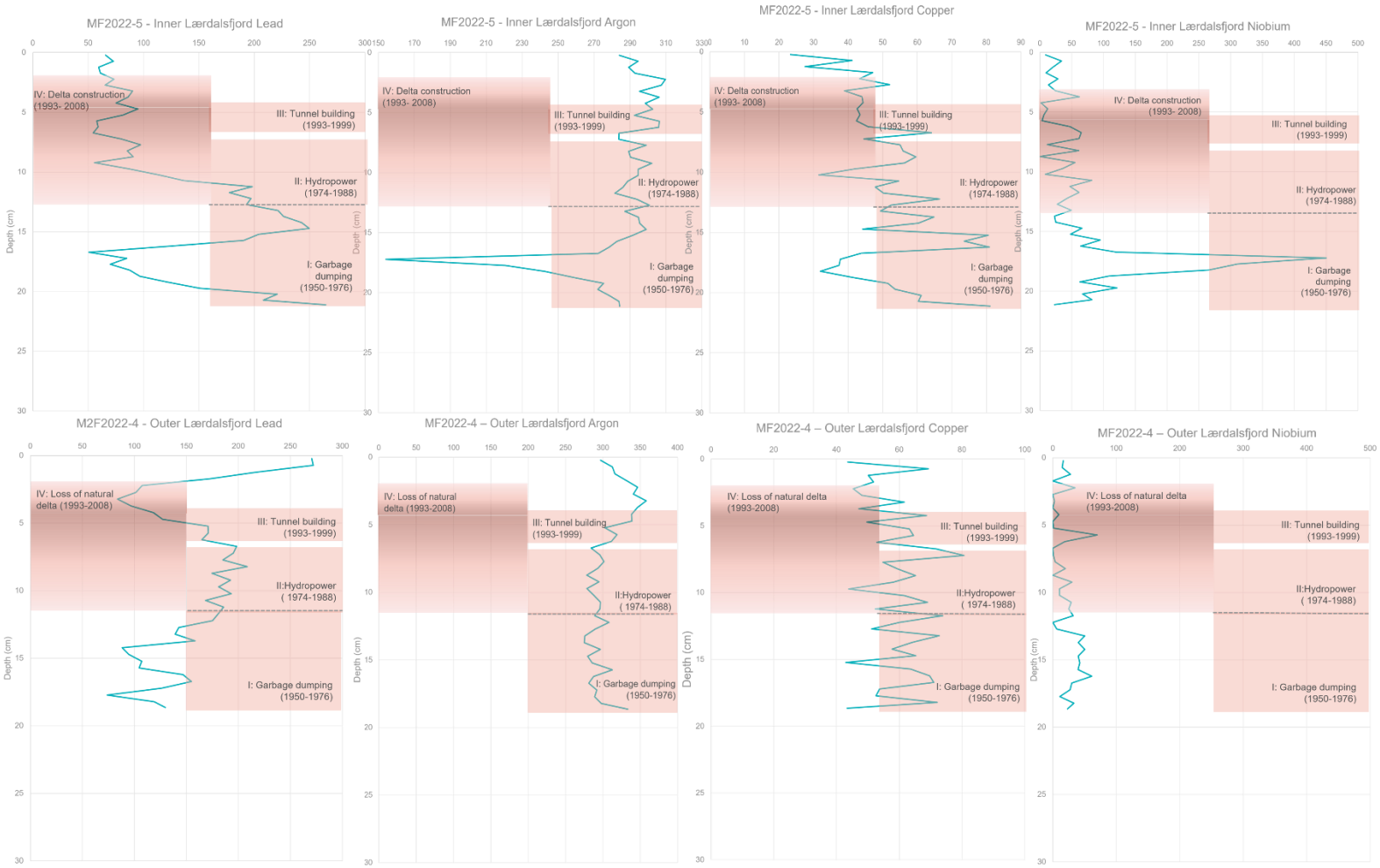

Figure 36, (top row) Lead, argon, copper, and niobium occurrences of the core MF2022-5 from the Inner Lærdalsfjord versus (bottom row) lead, argon, copper and niobium occurences of sediment core MF2022-4 from the Outer Lærdalsfjord.

6.2 Environmental significance of the sediment geochemistry in the Outer Lærdalsfjord

6.2.1 Polluting elements lead (Pb), argon (Ar), copper (Cu), and niobium (Nb) in the Outer Lærdalsfjord

The significant peaks of lead, argon, copper, and niobium of the Inner Lærdalsfjord are not visible in the same metal occurrences of the Outer Lærdalsfjord (Figures 37). A probable reason might be that the Outer Fjord is located more distant to the dumping site and thus might not get affected.

6.2.2 Bromine (Br) and lead (Pb)

In the Outer Lærdalsfjord, bromine and lead are following a nearly identical pattern for the entire depth-profile of the sediment core (Figure 38).

Heavy metals tend to be bound to organic material and fine grain sizes (Salomon and Forstner, 1988). The correlation between lead (red) and bromine (blue) (Figure 38) shows that the appearance of lead depends on the primary production of the fjord, represented by bromine. The more marine organic matter is produced, the more lead can be bound and sink down to the ground, due to the formation of bigger and thus heavier aggregates (Salomon and Forstner, 1988, Hongtao et al., 2010). Thus, it might be possible that there is generally no more lead input to the outer fjord, and that only the mode of sedimentation is changing according to the same processes indicated for the Inner Lærdalsfjord.

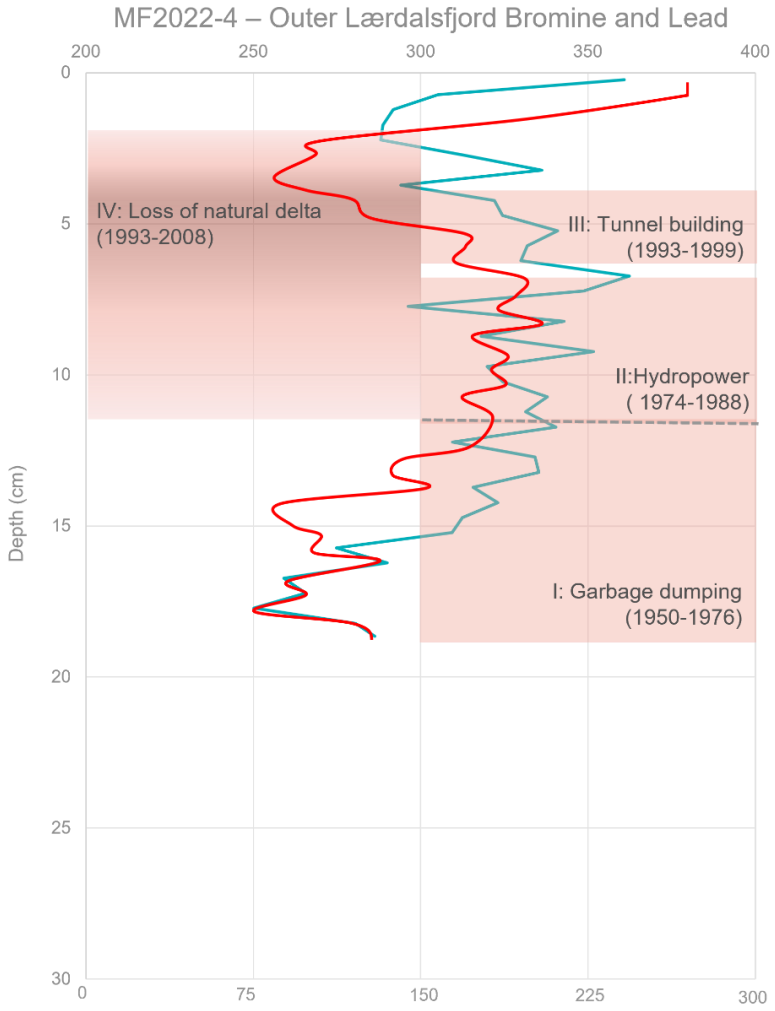

Figure 37, Outer Lærdalsfjord, bromine (blue) on top of lead (red). The upper x-scale resembles the bromine values. The lower x-scale resembles the lead values.

6.2.2 General geochemistry and magnetic susceptibility

The geochemical record of the Outer Lærdalsfjord is less influenced by the events of environmental change (Table 1) than the geochemical record of the Inner Lærdalsfjord. The Outer fjord is shielded from the causes of environmental impact due to three reasons:

1) The Outer Lærdalsfjord is located more distant to the events of interest and thus not directly influenced by these like it is the case in the Inner Lærdalsfjord.
2) The Outer Lærdalsfjord is separated by a sill from the Inner Lærdalsfjord. There is little to no exchange of organic matter, mineral matter, and pollutants between the Inner Lærdalsfjord and the Outer Lærdalsfjord. Thus, anthropogenic induced

accumulation of elements is most likely to be restricted to the Inner Lærdalsfjord rather than being transported into the Outer Lærdalsfjord basin.

3) The constant magnetic susceptibility signal from the Outer Lærdalsfjord (Figure 23) indicates sediment input from the same source for the entire time span of 80 years. This suggests that there was little to no interaction between Inner and Outer Lærdalsfjord sedimentation processes.

This indicates, that the Outer Lærdalsfjord is an independent fjord system with a different general geochemistry than the Inner Lærdalsfjord.

6.3 Environmental implications for the Lærdalsfjord

There are differences within the geochemical composition of the Inner Lærdalsfjord and the Outer Lærdalsfjord. To elaborate and visualize these differences between both fjord basins, a simple illustrational box model is created (Figure 39).

The model shows the input to the Inner Lærdalsfjord, including the events of *Phase I (Garbage dumping), II (Hydropower), III (Rock dumping), and IV (Delta construction)* that influence the amount and type of pollutants, mineral matter, and organic matter being transported into the fjord. Divided by a sill, the Outer Lærdalsfjord shows a less heavy impact on this material compared to the Inner Lærdalsfjord. The Outer Lærdalsfjord receives an additional input of mineral and organic matter through the river Erdalselv (Figure 39).

Both fjord basins resemble the overall relationship between the same elemental occurrences, indicating the respective effect of environmental change to each fjord basin independently. It shows the Inner Lærdalsfjord being more affected by environmental change and the respective events compared to the Outer Lærdalsfjord. Additionally, it indicates that each fjord basin has its own cycle and only influences each other little.

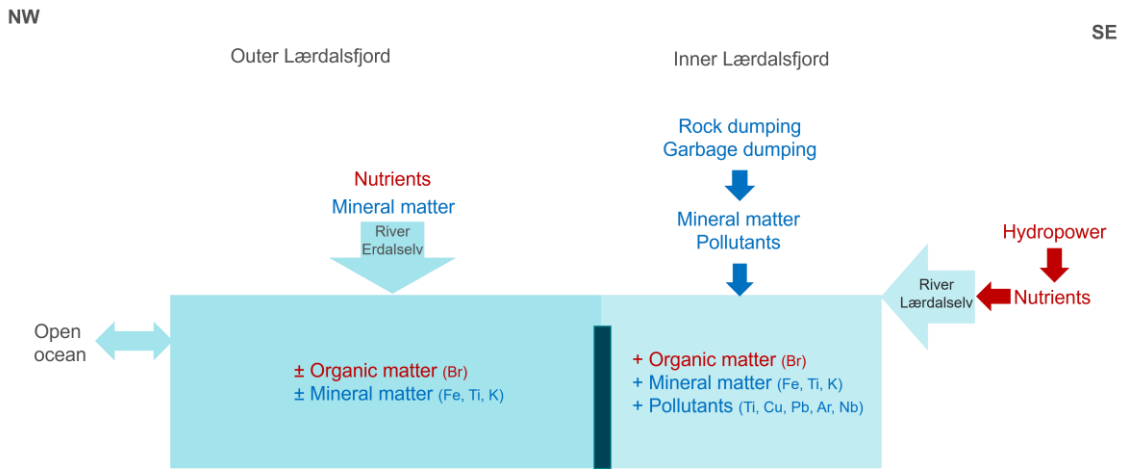

Figure 38. Box model of the Lærdalsfjord. The left side shows the input to the Outer Lærdalsfjord basin by the river Erdalselv. The right side shows the inputs to the Inner Lærdalsfjord by the river Lærdaslelv and rock and garbage dumping. Each fjord basin shows their respective fractions of organic matter, mineral matter and pollutants, which are either increasing (+), or stable (±) in relation to each basin.

7. Conclusion

The geochemical record of the sediments shows differences between the Inner and the Outer Lærdalsfjord.

Changes within elemental occurrences in the sediments can be traced back to their respective cause of environmental change.

The geochemical data suggest that the Lærdalsfjord should be differentiated into two independent systems, the Inner Lærdalsfjord and the Outer Lærdalsfjord. Thus, any conclusions about the fjord environment and its health status should be assessed for the Inner and the Outer Lærdalsfjord basin independently.

The EU Water Framework Directive should not classify the environmental condition of the entire Lærdalsfjord based on results from one fjord basin only.

The geochemical data set suggest that only the Inner Lærdalsfjord basin is heavily affected by environmental change that took place throughout the past 80 years. The Outer Lærdalsfjord seems to be almost unaffected by the same environmental conditions.

8. References

- Ahmed, A. Y., Abdullah, P., Wood, A. K., Hamza, M. S., Othman, M. R. (2013). Determination of some trace elements in marine sediment using ICP-MS and XRF: A comparative study. *Oriental Journal of chemistry, Volume 29* (2), pp. 645-653. Determination of some trace elements in marine sediment using ICP-MS and XRF (orientjchem.org)
- Aksnes D. I., Aure J., Johansen P-O., Johnsen G. H., Salvanes A. G. V. (2019). *Multi-decadal warming of Atlantic water and associated decline of dissolved oxygen in a deep fjord*. Estuarine, Coastal and Shelf Science, Volume 228. https://doi.org/10.1016/j.ecss.2019.106392
- Bianchi T., Arndt S., Austin W., Benn D., Bertrand S., Cui X., Faust J., Koziorowska-Makuch K., Moy C., Savage C., Smeaton C., Smith R., Syvitski J. (2020). *Fjords as Aquatic Critical Zones (ACZs)*. Earth-Science Reviews, Volume 203. https://doi.org/10.1016/j.earscirev.2020.103145
- Bjerknes V. , Raddum G. (2001). E19 Tunnel Aurland – Lærdal. *Registrering og overvaking av vasskvalitet, botndyr og fisk i Lærdalselva og Kuvella frå 1994 til 2000*. Samlerapport. NIVA 4409-2001.https://niva.brage.unit.no
- Coassin M., Ursini F., Bindoli A. (1992). *Antioxidant effect of manganese*. Archives of Biochemistry and Biophysics. Volume 299 (2), pp. 330-333. https://doi.org/10.1016/0003-9861(92)90282-2
- Croudace, I., Rindby, A., Rothwell, R. (2006). *ITRAX: Description and Evaluation of a New Multi-Function X-ray Core Scanner*. Geological Society, London, Special Publications. Vol 267, pp. 51-63. http://dx.doi.org/10.1144/GSL.SP.2006.267.01.04
- Dale, T., 2023, *personal communication*.
- Delmonte D., Gori C., Lambruschi E., Mantovani L., Mezzadri F., Bersani D., Lottici PP., Gilioli E., Solzi M., Tribaudino M. (2018): *A comprehensive study of the magnetic properties of the pyroxenes series CaMgSi2O6-Co2Si2O6 as a function of Co content*. Journal of Physics Condensed Matter 30 (28): 285801. Epub 2018 Jun 4. PMID: 29863483. https://doi.org/10.1088/1361-648x/aaca0e
- European Comission (2023). *Water Framework Directive*, Department of Environment. Water Framework Directive (europa.eu) . Retrieved 09.04.2023
- Gjelle S., Sigmond M.O. E. (1995). *Bergartsklassifikasjon og kartfremstilling*. Norges Geologiske Undersøkelse (NGU). Vol 113.
- Gjerdingen, H. S. (2018*). Identifisering av flomavsetninger i fjorder på Vestlandet - Aurlandsfjorden og Lærdalsfjorden*. MSc. Thesis, Universitet i Bergen.

- Haflidason H. (2020). Marine Geological Cruise Report. *Investigating the flood- and deglaciation history recorded in the sediments of Lærdalsfjorden, Western Norway*. University of Bergen, Department of Earth Science.
- Hauge L., 2023, personal communication
- Heggøy E., Johansen P-O., Johannessen P. (2007). *Marinbiologisk miljøundersøkelse i Lærdalsfjorden i 2006*. Universitetsforskning Bergen (UNIFOB), Rapport, nr. 6 – 2007.
- Howe J.A., Austin W.E.N, Forwick M., Paetzel M. (2010): *Fjord systems and Archives*. Geological Society of London, Volume 344. https://doi.org/10.1144/SP344
- Hongtao Z., Xuyong L., Xiaomei W., Di T. (2010): *Grain size distribution of road-deposited sediment and its contribution to heavy metal pollution in urban runoff in Beijing, China*, Journal of Hazardous Materials, Volume 183, Issues 1–3, Pages 203-210. https://doi.org/10.1016/j.jhazmat.2010.07.012.
- Howarth, R. J. & Sinding-Larsen, R. (1983). *Multivariate analysis*. In: R. J. Howarth (ed.): Statistics and data analysis in geochemical prospecting. Elsevier Science, Amsterdam, 207-289. https://doi.org/10.1016/B978-0-444-42038-1.50012-5
- Jensen T., Stensby K. S., Vognild I. H, Brittain J. E. (2021): Norwegian Water Resources and Energy Directorate (NVE). *Norway's hydroelectric development 1945 – 1990.* Rapport, 28/2021. NVE Rapport
- Johannessen P. J., Lønning T. M. (1988). *Resipientundersøkelser i Lærdal kommune*. Institutt for Marinbiologi. Rapport, 70/1988.
- Johnsen T. M., Golmen L. G. (1992). *Konsekvensanalyse ay duming av tunnelmasse i sjøen i Lærdalsområdet.* NIVA-Rapport O-92144, Norsk institutt for vannforskning.
- Klima- og miljødepartementet (1976): *Miljøvernkonvensjon av 19. februar 1974, mellom Danmar, Finland, Norge og Sverige*. https://lovdata.no/dokument/NL/lov/1976-04-09-21
- Kuhlmann H., Freudenthal T., Helmke P., Meggers H. (2004). *Reconstruction of paleoceanography off NW Africa during the last 40,000 years: influence of local and regional factors on sediment accumulation*. Marine Geology, 207(1-4), pp. 209-224. https://doi.org/10.1016/j.margeo.2004.03.017
- Lærdal municipality (1991): *Regulation plan for Grandane. Plan archive*, Lærdal municipality.
- Lærdal municipality (1995): *Partly revision of the regulation plan for Grandane from 1991*. Plan archive, Lærdal municipality.

- Lærdal municipality (2005): *Regulation plan for "Ytre Grandane og Habben".* Plan archive, Lærdal municipality.
- Le Maitre, R., Streckeisen, A., Zanettin, B., Le Bas, M., Bonin, B., & Bateman, P. (2002). *Igneous Rocks: A Classification and Glossary of Terms: Recommendations of the International Union of Geological Sciences Subcommission on the Systematics of Igneous Rocks*. Cambridge University Press, 2nd edition. https://doi.org/10.1017/CBO9780511535581
- Miserocchi S., D'Angelo A., Del Bianco F., Giglio F., Langone L., Tesi T., Aliani S. (2016). Modern sediment distribution and composition within the Kongsfjorden, Svalbard Islands. *ARCA Final Report*. Abstract Miserocchi ARCA final (arcaproject.it)
- Møller, H. S., Jensen, K. G., Kuijpers, A., Aagaard-Sørensen, S., Seidenkrantz, M.-S., Prins, M., Endler, R., Mikkelsen, N. (2006). Late-Holocene environment and climatic changes in Ameralik Fjord, southwest Greenland: evidence from the sedimentary record. The Holocene, 16(5), pp. 685–695. https://doi.org/10.1191/0959683606hl963rp
- Munsell Soil colour chart. Soil Color Charts Book Includes Over 10 Munsell Soil Color Charts | Munsell Color System; Color Matching from Munsell Color Company
- Niemistö, L. (1974). A gravity corer for studies of soft sediments. Merentutkimuslait Julk/ Havsforskningsinstituttets Skrifter, 238, pp. 33–38
- Norgeskart.no https://www.norgeskart.no/
- Norgeibilder.no https://www.norgeibilder.no/
- NORCE Laboratorium for ferskvannsøkologi og innlandsfiske (LFI), (2019): Kartlegging av elvebunnen i Lærdalselva April 2019. *Har tilførte masser fra kommen høsten 2018 påvirka elvebunnen?* Rapport 335.
- Norskklimaservicesenter. Observasjoner og værstatistikk - Seklima (met.no) retrieved 02.05.2023.
- Norwegian Water Resources and Energy Directorative (NVE). Vannkraftdatabase - NVE Retrieved 11.04.2023.
- Østfold Energi (2023). *Vannkraft – Kraftverk i Vestland.* Kraftverk i Vestland - Østfold Energi (ostfoldenergi.no) . Retrieved 10.04.2023.
- Paetzel M., Dale T. (2010). *Climate proxies for recent fjord sediments in the inner Sognefjord region, western Norway*. Geological Society, London, Special Publications. Vol. 344, pp. 271-288. https://doi.org/10.1144/SP344.19
- Porten.no (Halvor F. Storvik). Han kan feira 25 ar med camping i Lærdal. Han kan feira 25 år med camping i Lærdal (porten.no) (20.05.2018). Retrieved 01.05.2023.

- Rebolledo L., Sepúlveda J., Lange C.B., Pantoja S., Bertrand S., Hughen K., Figueroa D. (2008). Late Holocene marine productivity changes in Northern Patagonia-Chile inferred from a multi-proxy analysis of Jacaf channel sediments, *Estuarine, Coastal and Shelf Science*, Volume 80(3), pp. 314-322. https://doi.org/10.1016/j.ecss.2008.08.016
- Ren J., Jiang H., Seidenkrantz M-S., Kuijpers A. (2009). A diatom-based reconstruction of Early Holocene hydrographic and climatic change in a southwest Greenland fjord. Marine Micropaleontol, Volume 70(3-4), pp. 166–176. https://doi.org/10.1016/j.marmicro.2008.12.003
- Rodríguez-Germade I., Rubio B., Rey D. (2014). XRF scanners as a quick screening tool for detecting toxic pollutant elements in sediments from Marín harbour in the Ría de Pontevedra (NW Spain), *Marine Pollution Bulletin*, Volume 86(1-2), 458-467. https://doi.org/10.1016/j.marpolbul.2014.06.029
- Rothwell, R., Croudace, I. (2015). Twenty Years of XRF Core Scanning Marine Sediments: What Do Geochemical Proxies Tell Us? In: Croudace, I., Rothwell, R. (eds) Micro-XRF Studies of Sediment Cores. Developments in Paleoenvironmental Research, vol 17. Springer, Dordrecht. https://doi.org/10.1007/978-94-017-9849-5_2)
- Ruiz F. (2001). Trace Metals in Estuarine Sediments from the Southwestern Spanish Coast, *Marine Pollution Bulletin*, Volume 42(6), 481-489. https://doi.org/10.1016/S0025-326X(00)00192-2
- Salomon W, Forstner U (1988): Pollution of the North Sea: An Assessment. Springer Verlag, Berlin. http://dx.doi.org/10.1007/978-3-642-73709-1
- Seki, A., Tada, R., Kurokawa, S., Murayama M. (2019). High-resolution Quaternary record of marine organic carbon content in the hemipelagic sediments of the Japan Sea from bromine counts measured by XRF core scanner. *Progress in Earth and Planetary Science,* 6(1). https://doi.org/10.1186/s40645-018-0244-z
- Statens vegvesen. Vei, trafikk, kjøretøy og førerkort | Statens vegvesen. Retrieved 12.04.2023.
- Statens kartverk (1961): Aerial photograph from Læredal WF-2223-L19.l
- Stigebrandt, A. (2012). *Hydrodynamics and Circulation of Fjords*. In: Bengtsson, L., Herschy, R.W., Fairbridge, R.W. Encyclopedia of Lakes and Reservoirs. Encyclopedia of Earth Sciences Series. Springer, Dordrecht, pp. 327 - 344. https://doi.org/10.1007/978-1-4020-4410-6_247
- Store Norske Leksikon (Knut A. Rosvold). *Borgund kraftverk.* Borgund kraftverk – Store norske leksikon (snl.no) (17.01.2021). Retrieved 10.04.2023.

- Syvitski J., Burrel D., Skei J. (1987). *Fjords: Processes and Products.* Springer. https://doi.org/10.1007/978-1-4612-4632-9
- Syvitski J., Shaw J. (1995). *Sedimentology and Geomorphology of Estuaries*, Developments in Sedimentology, Vol 53, Chapter 5, pp. 113-178. https://doi.org/10.1016/S0070-4571(05)80025-1
- Tyson R.V, Pearson T.H (1991). *Modern and Ancient Continental Shelf Anoxica.* Geological Society, Special Publication No 58, pp. 1 -24.
- Vann-Nett (2023). *Lærdalsfjorden*. VannNett-Portal (vann-nett.no). Retrieved 09.04.2023
- Yang Y. (2023). *The environmental signal of diatoms in recent (0 – 90 years) sediments from the Lærdalsfjord, Western Norway.* BSc. Thesis, Høgskulen på Vestlandet.

9. Appendix

Appendix 1: Construction plan of the delta from 1991, Lærdal municipality

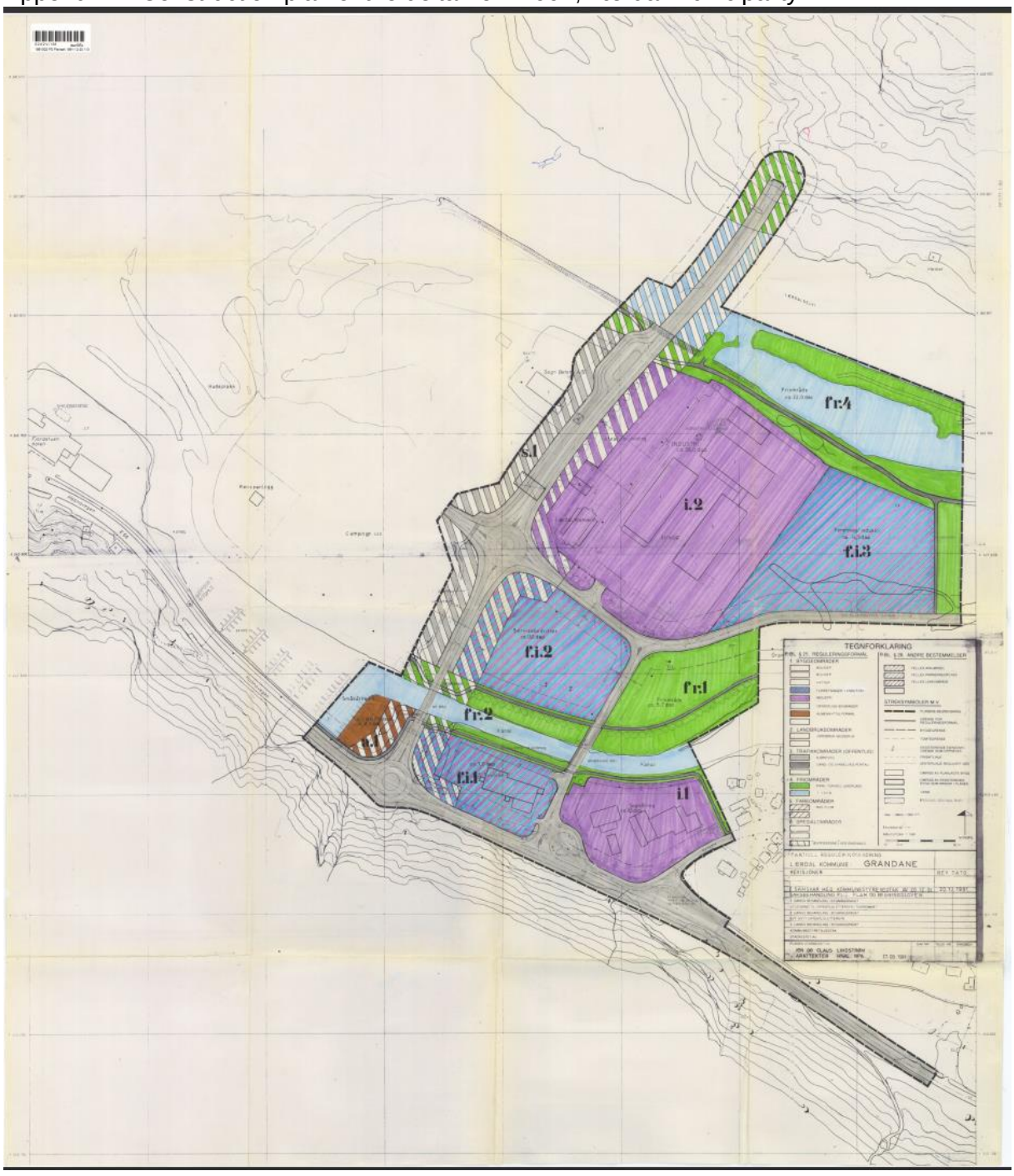

Appendix 2: Construction plan delta Lærdal municipality, 1995

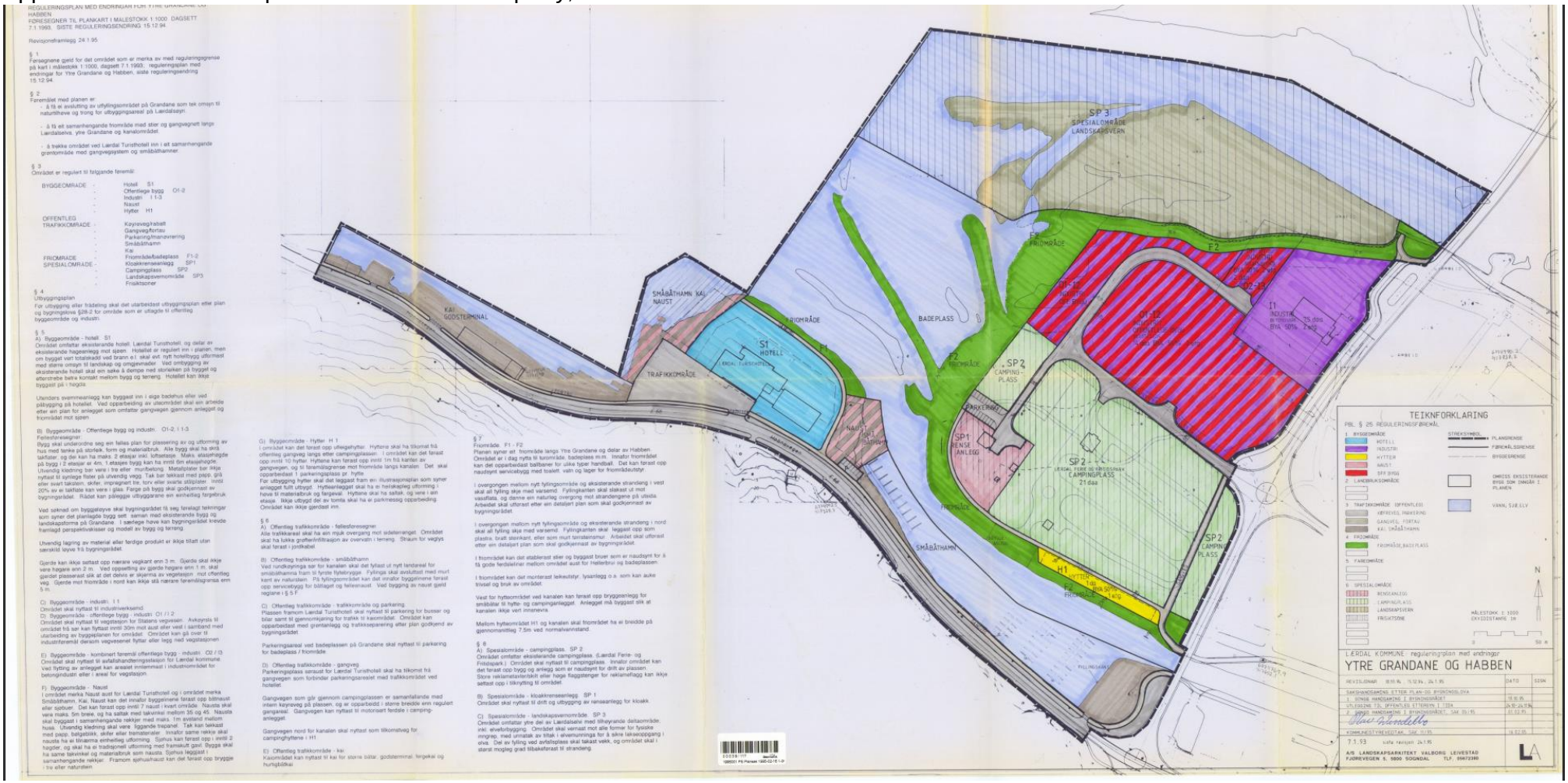

Appendix 3: Construction plan delta 2005, Lærdal municipality

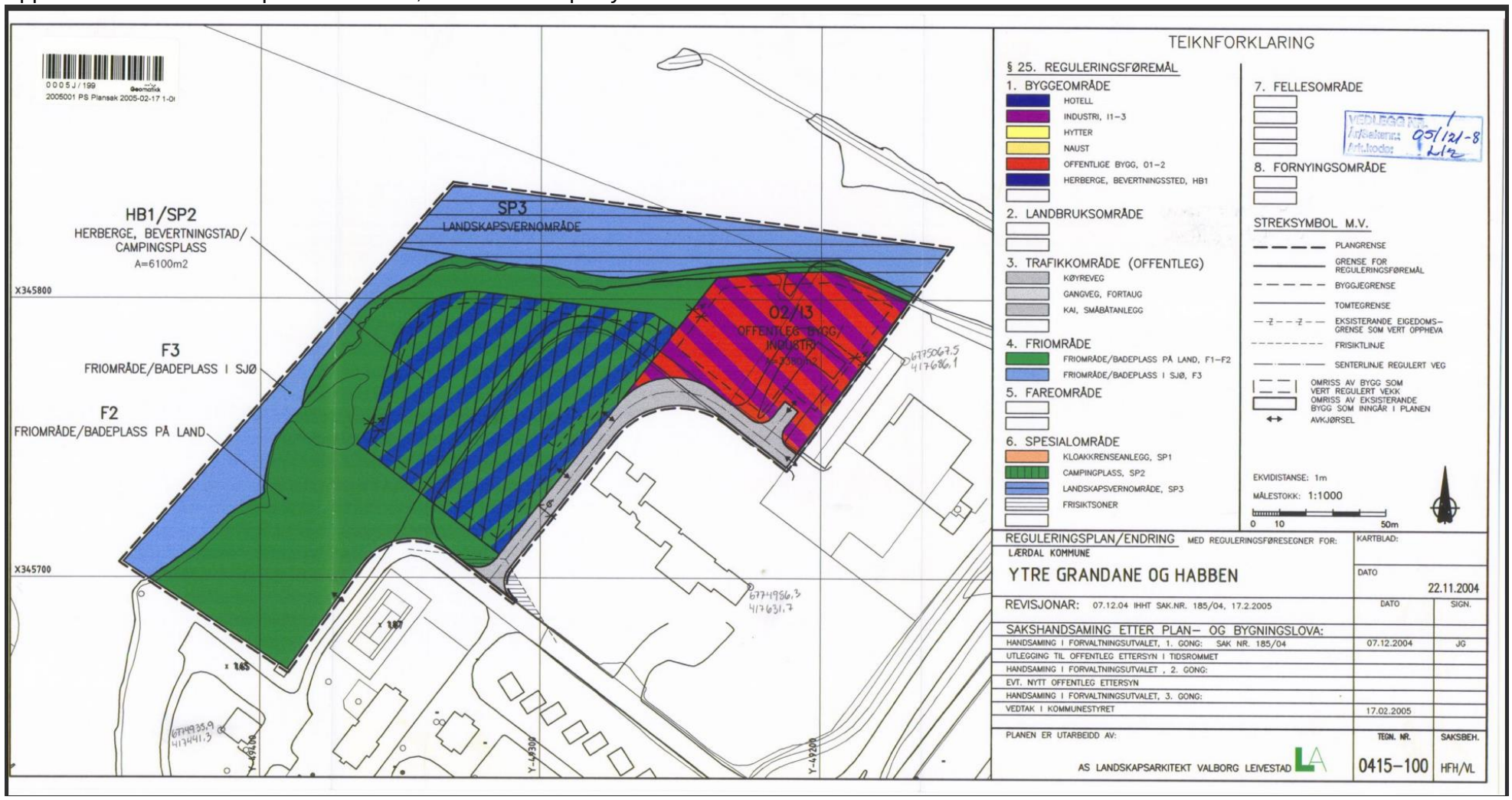

Appendix 4: Core MF2022-4 Statistical correlation

	Al	Si	P	S	Cl	Ar	K	Ca	Ti	V	Cr	Mn	Fe	Co	Ni	Cu	Zn	Ga	Se	Br	Rb	Sr	Y	Zr	Nb	Ba	La	Ce	Ta	W	Pb
Al	1,00																														
Si	0,13	1,00																													
P	-0,01	-0,04	1,00																												
S	0,02	0,04	-0,02	1,00																											
Cl	0,00	0,01	-0,04	0,42	1,00																										
Ar	-0,02	-0,34	0,11	-0,04	-0,30	1,00																									
K	0,12	0,72	-0,06	0,00	0,10	-0,29	1,00																								
Ca	0,14	0,72	-0,10	0,04	0,22	-0,38	0,82	1,00																							
Ti	0,14	0,59	-0,06	0,07	0,21	-0,35	0,75	0,77	1,00																						
V	0,05	0,15	-0,03	0,07	0,11	-0,18	0,21	0,22	0,18	1,00																					
Cr	0,01	0,20	-0,07	0,12	0,25	-0,15	0,27	0,29	0,22	0,02	1,00																				
Mn	0,11	0,50	-0,10	0,10	0,30	-0,38	0,65	0,69	0,68	0,27	0,18	1,00																			
Fe	0,14	0,65	-0,11	0,14	0,44	-0,50	0,82	0,85	0,78	0,24	0,34	0,75	1,00																		
Co	0,04	0,04	-0,02	0,05	0,12	-0,08	0,06	0,06	0,08	-0,06	0,04	0,06	0,12	1,00																	
Ni	0,02	0,08	-0,05	-0,10	-0,09	-0,07	0,09	0,11	0,08	0,00	0,01	0,17	0,07	-0,03	1,00																
Cu	0,03	0,10	-0,03	-0,04	0,06	-0,13	0,11	0,09	0,08	0,00	0,04	0,14	0,12	0,02	0,15	1,00															
Zn	0,05	0,26	-0,06	-0,02	0,02	-0,22	0,31	0,27	0,29	0,09	0,14	0,27	0,32	0,06	0,11	0,14	1,00														
Ga	0,01	0,13	-0,08	-0,12	0,03	-0,08	0,14	0,14	0,09	-0,04	0,04	0,12	0,15	0,10	0,10	0,26	0,10	1,00													
Se	0,11	-0,02	0,04	0,08	0,02	0,02	-0,03	-0,09	-0,09	0,03	-0,05	-0,12	-0,05	0,13	0,01	0,02	0,08	0,04	1,00												
Br	0,05	0,13	0,06	-0,11	-0,12	-0,04	-0,02	0,00	-0,02	-0,03	-0,07	-0,07	-0,04	-0,03	0,01	-0,01	0,07	0,09	0,22	1,00											
Rb	0,05	0,25	0,01	0,19	0,29	-0,20	0,37	0,37	0,39	0,11	0,18	0,32	0,43	0,03	0,02	0,04	0,12	0,06	0,01	-0,17	1,00										
Sr	0,10	0,24	-0,02	0,03	0,18	-0,23	0,35	0,41	0,39	0,17	0,14	0,43	0,43	0,03	0,07	0,11	0,26	0,13	-0,09	-0,07	0,33	1,00									
Y	-0,01	0,01	-0,07	0,03	0,01	-0,10	0,01	-0,01	-0,01	0,05	0,02	-0,05	0,02	0,11	-0,04	0,01	-0,01	-0,03	0,04	-0,02	-0,01	0,07	1,00								
Zr	0,00	0,07	0,05	0,01	-0,01	0,00	0,10	0,11	0,12	-0,01	-0,06	0,13	0,09	0,07	0,03	-0,04	0,05	0,05	-0,06	0,01	0,15	0,20	0,02	1,00							
Nb	-0,01	0,04	-0,07	0,04	0,11	-0,04	0,05	0,06	-0,01	0,02	0,10	0,01	0,08	-0,02	0,00	0,05	0,00	0,07	-0,09	0,02	0,07	0,01	-0,09	-0,03	1,00						
Ba	-0,02	0,14	0,02	0,00	0,02	0,01	0,21	0,20	-0,02	-0,04	0,26	0,06	0,15	0,03	-0,06	-0,01	-0,01	0,03	-0,06	-0,09	0,12	0,09	-0,03	-0,05	0,13	1,00					
La	0,10	0,14	-0,03	0,06	0,04	0,06	0,13	0,13	0,14	-0,23	-0,01	0,10	0,13	0,09	0,03	-0,01	0,01	0,04	-0,05	0,01	0,04	0,10	0,08	-0,05	-0,07	-0,11	1,00				
Ce	0,02	0,06	0,00	0,04	0,12	-0,07	0,16	0,15	0,29	-0,09	-0,16	0,22	0,17	-0,04	0,13	0,08	0,07	0,07	-0,01	0,09	0,09	0,08	0,00	0,10	-0,09	-0,58	0,21	1,00			
Ta	0,06	0,16	-0,02	0,14	0,36	-0,24	0,14	0,25	0,22	0,06	0,18	0,16	0,28	0,10	0,02	-0,27	0,09	-0,29	0,12	0,18	0,06	0,07	-0,10	-0,03	0,03	-0,06	0,09	0,13	1,00		
W	0,11	0,41	-0,06	0,14	0,37	-0,36	0,47	0,54	0,45	0,22	0,28	0,46	0,60	0,08	0,07	0,20	0,23	0,21	0,00	-0,01	0,33	0,30	0,03	0,09	0,08	0,11	0,06	0,08	0,14	1,00	
Pb	0,10	0,01	0,03	-0,14	-0,10	-0,20	-0,14	-0,09	-0,13	-0,02	-0,04	-0,13	-0,13	0,05	-0,03	0,13	0,12	-0,03	0,18	0,27	-0,09	-0,02	0,02	-0,04	0,01	-0,06	-0,08	-0,13	0,12	0,08	1,00

Appendix 5: Core MF2022-5 Statistical correlation

	Al	Si	P	S	Cl	Ar	K	Ca	Ti	V	Cr	Mn	Fe	Co	Ni	Cu	Zn	Ga	Se	Br	Rb	Sr	Y	Zr	Nb	Ba	La	Ce	Ta	W	Pb
Al	1,00																														
Si	0,18	1,00																													
P	0,17	0,08	1,00																												
S	0,19	0,11	0,13	1,00																											
Cl	0,11	-0,08	0,07	0,35	1,00																										
Ar	0,04	0,04	0,06	0,03	-0,19	1,00																									
K	0,12	0,74	0,04	0,04	-0,08	0,22	1,00																								
Ca	0,14	0,77	-0,01	0,08	0,08	0,11	0,82	1,00																							
Ti	0,13	0,62	0,04	0,00	0,06	0,14	0,80	0,75	1,00																						
V	0,03	0,13	0,06	0,05	-0,05	-0,02	0,15	0,14	0,09	1,00																					
Cr	-0,06	0,23	-0,06	0,16	0,17	0,03	0,21	0,24	0,16	0,03	1,00																				
Mn	0,07	0,57	-0,01	0,06	0,15	0,05	0,67	0,67	0,66	0,13	0,23	1,00																			
Fe	0,13	0,55	-0,01	0,08	0,14	0,19	0,83	0,71	0,78	0,15	0,23	0,68	1,00																		
Co	0,06	-0,14	-0,02	-0,04	0,05	-0,15	-0,15	-0,18	-0,14	-0,01	-0,05	-0,06	-0,14	1,00																	
Ni	-0,02	0,11	-0,11	-0,01	0,00	-0,02	0,06	0,10	0,05	0,01	0,12	0,17	0,05	-0,18	1,00																
Cu	-0,04	0,23	-0,08	0,01	0,05	0,06	0,25	0,25	0,20	0,00	0,09	0,26	0,17	-0,02	0,18	1,00															
Zn	0,05	0,30	-0,02	-0,03	0,14	0,03	0,41	0,43	0,45	0,12	0,10	0,39	0,49	-0,02	0,11	0,17	1,00														
Ga	-0,06	0,05	0,01	-0,03	0,01	0,02	0,06	0,09	0,08	0,00	0,08	0,10	0,13	0,09	0,05	0,35	0,13	1,00													
Se	-0,01	0,09	0,10	0,05	-0,01	0,03	0,07	0,04	0,03	0,04	-0,03	0,03	0,03	-0,04	0,05	0,05	0,10	0,15	1,00												
Br	-0,05	-0,06	-0,04	0,12	0,26	-0,07	-0,12	0,06	-0,06	-0,09	0,08	-0,02	-0,05	-0,09	0,01	0,06	0,02	0,00	0,10	1,00											
Rb	0,10	0,19	0,05	0,08	0,08	0,01	0,27	0,22	0,23	0,08	0,02	0,19	0,32	-0,02	0,03	0,08	0,22	0,09	0,10	-0,07	1,00										
Sr	0,12	0,11	0,01	0,03	0,30	-0,23	0,32	0,25	0,34	0,09	0,00	0,24	0,43	0,06	0,00	0,08	0,39	0,03	0,09	0,00	0,32	1,00									
Y	-0,06	0,07	0,01	-0,02	0,05	-0,09	0,06	0,07	0,09	-0,05	0,04	0,10	0,03	0,05	-0,02	0,06	-0,01	0,04	0,04	0,03	-0,09	0,12	1,00								
Zr	0,02	0,16	-0,06	0,06	0,18	-0,16	0,11	0,18	0,14	0,01	0,10	0,15	0,07	-0,02	0,09	0,05	0,08	-0,04	0,05	0,01	0,09	0,22	0,12	1,00							
Nb	0,06	0,04	0,02	-0,03	0,16	-0,54	-0,12	-0,01	-0,07	-0,05	-0,05	0,00	-0,15	0,08	0,06	-0,07	0,03	-0,08	0,04	0,02	0,01	0,14	0,15	0,21	1,00						
Ba	-0,01	0,14	0,02	-0,04	-0,20	0,15	0,27	0,13	0,07	0,00	0,06	0,04	0,21	0,04	0,01	0,02	0,03	0,07	0,12	-0,16	0,07	0,13	-0,05	-0,03	-0,08	1,00					
La	0,04	0,12	0,09	0,00	0,06	0,09	0,17	0,15	0,16	-0,22	-0,01	0,14	0,12	-0,05	0,02	0,07	0,05	-0,08	-0,04	0,02	0,06	0,03	0,06	0,05	-0,03	-0,06	1,00				
Ce	0,03	0,09	0,02	0,07	0,20	0,04	0,16	0,17	0,26	0,02	-0,10	0,27	0,22	-0,13	0,06	0,05	0,19	0,00	-0,03	0,04	0,09	0,10	-0,05	0,06	0,01	-0,49	0,11	1,00			
Ta	0,08	0,04	-0,03	0,20	0,39	-0,07	-0,01	0,11	0,01	0,01	0,15	0,06	0,06	-0,07	0,03	-0,32	0,08	-0,34	0,04	0,27	0,03	0,03	-0,07	0,14	0,08	-0,14	-0,05	0,12	1,00		
W	0,08	0,44	-0,05	0,21	0,35	0,00	0,40	0,57	0,39	0,09	0,34	0,49	0,43	-0,04	0,08	0,28	0,31	0,24	-0,02	0,22	0,15	0,10	0,01	0,15	0,02	-0,04	0,02	0,19	0,25	1,00	
Pb	0,02	0,40	0,00	0,07	0,08	0,03	0,30	0,40	0,31	0,12	0,18	0,31	0,23	-0,08	-0,03	0,20	0,29	0,06	0,08	0,04	0,13	0,08	0,02	0,15	-0,02	0,01	-0,09	0,10	0,15	0,43	1,00